Correlation between tensile ductility and impact properties of oxide dispersion-hardened ODS-Ta-W alloys

D. Preininger
Forschungszentrum Karlsruhe, Institute for Materials Research I, D-76021 Karlsruhe, P.O. Box 3640, Germany

Abstract

The effects of dispersion strengthening and grain refinement to the nano-crystalline level (d_k>3 nm) on the tensile ductility and Charpy-impact behaviour have been examined for ODS-Ta≤40at% W and ODS-W alloys by deformation/fracture models. Grain refinement strongly increases the ductile-to-brittle transition temperature DBTT and reduction of upper shelf energy U=ΔUSE/USE_o at constant fracture stresses and also reduces uniform ductility. Dispersion hardening increases further DBTT and energy shift U but additionally increases uniform ductility more pronounced at a nanoscale optimum particle size of d_p*≤5-40 nm. That reduces with increasing grain refinement, W alloying and decreasing particle volume fraction. A grain refinement-induced increase of fracture stresses as observed in W up to the size d_k≅ 500 nm, however, strongly reduces DBTT and weaker also energy shift U within the ultra-fine(uf) grain region. Minima in DBTT and shift U result at optimum uf grain sizes d_k≥50 nm already at a weak fracture stress increase, which increase with increasing W alloying and dispersion hardening. The deduced optimum W content for ductile and high strengthened ODS-Ta-W alloys are between 20-≤40at% W dependent on dispersion strengthening, grain refinement and induced fracture stress increase.

1. Introduction

Oxide dispersion-strengthened (ODS)-Ta-W alloys due to their high ductility, strength and excellent impact properties are generally proposed as low (<20°C) and high-temperature structural materials for application up to 1300°C. These, besides the more brittle W alloys are especially discussed for application as structural material of the divertor of future fusion reactors to control heat and particles (hydrogen isotopes, helium and impurities) from plasma at operational temperatures of ≤1200-1300°C. High thermal shock, strength and conductivity properties are required for that application together with a reduced hydrogen and helium embrittlement. For comparison, the use of the high strengthened ferritic-martensitic ODS-(7-13)CrWVTa steels is restricted below < 750°C. For optimisation of this ductile, high-strengthened ODS-Ta-W and ODS-W alloys, the superimposed effects of dispersion strengthening and grain refinement to the nano-crystalline (nc) level (d_k>3 nm) on the tensile ductility and Charpy-impact behaviour have been examined by micro-mechanical deformation and ductile/dynamic fracture models [1]. Especially, the effects of dispersion parameters as mean size and volume fraction upon the grain size dependence of the ductile-to-brittle transition temperature DBTT and ductile upper shelf impact energy USE have been investigated taken into account strengthening by ≤40at.% W solid solution alloying and irradiation-induced defect formation. Additionally, also the influence of a combined increase of ductile and dynamic fracture stresses due to grain refinement has been considered which might result from a transition of deformation process from dislocation glide to diffusion-induced grain-boundary sliding. The data used for predictions have been observed by analysing the reported work-hardening behaviour of large grained Ta-(0-20)W alloys [2] and the ultra-fine (uf) grained pure Ta [3] produced by the equal channel angular pressing (ECAP). The predictions are particularly compared with the behaviour for ODS-(7-13)CrWVTa steels and reported results upon the grain refinement effects of the DBTT for pure W [4].

2. Model for the influence of dispersion hardening and grain refinement on tensile ductility and impact behaviour of ODS-Ta-W alloys

The total yield strength of ODS metals is given by the linear superposition

$$\sigma_y = \sigma_{dk} + \Delta\sigma_p + \Delta\sigma_i \qquad (1a)$$

from various contributions like grain boundaries, σ_{dk}, incoherent dispersions or non-shearable precipitates, $\Delta\sigma_p$, and additionally from small defects $\Delta\sigma_i$ as atomic clusters (<1 nm), dislocation loops and helium bubbles (>1 nm) formed in the case of neutron irradiation within the matrix. Grain boundary strengthening is described by the well-known Hall-Petch relation

$$\sigma_{dk} = \sigma_{o,m} + k_{HP} / d_K^{1/2} \qquad (1b)$$

dependent on the material constant k_{HP} and the mean grain size d_K together with the solid solution contribution $\sigma_{o,m}$ depending on alloying as the W content in Ta-W alloys. It is generally valid for metals up to nc grain sizes of $d_K \cong$3-20 nm [5] as about ≈3.4 nm for iron. Strengthening due to incoherent particles or larger coherent precipitates above their shearable limit can be expressed according to the Orowan dislocation by-pass process [1] by

$$\Delta\sigma_p = \beta_{OR}\, \mu\, b\, M\, (f_v)^{1/2}/d_p \qquad (2)$$

with the coefficient $\beta_{OR}=1/(2\Pi)\, \ln\{d_p[\Pi/(6\, f_v)]^{1/2}/b\}$ for screw dislocations. Here, f_v is the volume fraction of uniform distributed particles of mean diameter d_p in parallel glide planes, μ the shear modulus, b the Burgers vector and M≈2.73 the Taylor factor describing texture. Dynamic fracture as observed from Charpy-impact tests is assumed to occur stress-induced by micro-crack formation within a local damage area of plastic the crack-zone before the main crack. It instable propagates, if the triaxial stress locally exceeds dynamic fracture stress σ_f at strain rates of order $\varepsilon` = 10^3\ s^{-1}$. Brittle fracture then appears below the ductile to brittle transition temperature DBTT corresponding to the condition for the uniaxial yield strengths $\sigma_y(T=DBTT) \geq \sigma_f^* = \sigma_f/k_I$, where k_I denotes the stress intensity at this local fracture area. Taking into account the temperature (T) and strain rate ($\varepsilon`$) dependence of thermally activable yield strength $\sigma_e(T,\varepsilon`) = P \exp(-\beta_d T)$ [6] together with their athermal component $\sigma_o=\sigma_{dk}+\Delta\sigma_p+\Delta\sigma_i$, the transition temperature DBTT can be expressed by [1,7a]

$$DBTT = - (1/\beta_d) \ln[(\sigma_f^* - \sigma_o)/ P] \qquad (3)$$

dependent on maximum thermal yield stress P (Peierls stress) at T=0 K and the material coefficient $\beta_d = \beta_o - \beta_1 \ln \varepsilon`$ with their constants β_o, β_1. For calculations of Ta-≤40W, the coefficients $\beta_o=5.35\ 10^{-3}\ K^{-1}$, $\beta_1=3.27\ 10^{-4}\ K^{-1}$ [5,6] with P=1125 MPa [6,8,9] as observed for tantalum have been used. The strength-induced, relative increase of initial $DBTT_o$ according to eq. 3 can be in approximation described by $V=\Delta DBTT/DBTT_o \cong (K_d/P)\Delta\sigma_o$ for lower strengths $\Delta\sigma_o$, where the constant $K_d \leq e=2.718$ is only weakly dependent on T, $\varepsilon`$. This approximation which gives $K_d/P \cong 0.00278\ MPa^{-1}$ for the reduced activation ferritc-martensitic (RAFM)-(7-9)CrWVTa steels agree about with the DBTT shift $\Delta DBTT=K\Delta\sigma_i$, $K \cong 0.6\ MPa^{-1}$ deduced from 3-dimensional FEM calculations [10] of plasticity within the damage zone of crack for the similar 7CrWVTa(RAFM) steel F82H in dependence of irradiation strengthening $\Delta\sigma_i$, measured at the irradiation equal test temperature of

T_{irr}=T=300°C. Ductile rupture described by the upper shelf energy USE of Charpy-tests is assumed to occur by strain-induced damaging through void formation and their coalescence within the local fracture zone. Fracture appears if the local stress within the critical damage zone achieves the ductile fracture stress $\sigma_y=\sigma_{fd}/k_I \geq \sigma_f^*$ or at least a critical fracture strain ε_f corresponding to a critical damage. The upper shelf energy USE $\propto w_f$ is proportional to the deformation work w_f done over the whole volume of plastic damage zone up to fracture appearance. The calculation of w_f takes into account the yield strength dependence of plastic zone size $r_p \propto 1/\sigma_y^2$ [11] together with the local work-hardening $\sigma(\varepsilon)$ and stress intensity within the critical damage zone of instable micro-crack nucleation at position x_f according to the micro-mechanical deformation model described in [1]. A yield strength increase reduces r_p and critical distance x_f of fracture initiation to the main crack tip as well as the stress intensity k_I. From this model, the relative reduction of upper shelf energy $U_p=\Delta USE_p/USE_o$ normalized to the initial value USE_o for example due to dispersion strengthening $\Delta\sigma_p$ can be analytically expressed by

$$U_p = \Delta USE_p/USE_o = 1 - \phi\, [1/(1+\Delta\sigma_p/\sigma_y)]\, (\varepsilon_f^p/\varepsilon_f)\, C_L \qquad (4)$$

$$C_L = \frac{\{1+ \Delta\sigma_{\varepsilon,m}^p/(\sigma_y+\Delta\sigma_p)-[\sigma_{fd}^{*p}/(\sigma_y+\Delta\sigma_p)-1]/(\varepsilon_f^p R_m)\}}{\{1+ \Delta\sigma_{\varepsilon,m}/(\sigma_y)-[\sigma_{fd}^{*}/\sigma_y -1]/(\varepsilon_f R_m)\}}$$

in dependence of main microstructural parameters as f_v and d_p. The fracture mechanical coefficient $\phi \cong 1$ which describes the strength-induced change of plastic strain distribution $\varepsilon(x)$ can be obtained from comparison of eq.4 with FEM calculations. Here, $\Delta\sigma_{\varepsilon,m}$ and $\Delta\sigma_{\varepsilon,m}^p$ denote the maximum strain hardening at $\varepsilon \rightarrow \infty$ for the initial (f_v=0) and dispersion-strengthened state f_v, d_p and ε_f, ε_f^p the corresponding local fracture strains dependent on the relevant ductile fracture stresses σ_{fd}^*,σ_{fd}^{*p} and $R_m(T,\varepsilon`)=RM/b \geq 1$ [1] the normalized dislocation annihilation coefficient, where mobile dislocations spontaneously annihilated at achieve of the critical capture radius distance $R \geq b$. At least fracture appears at achieve of a critical fracture strain of ε_f =0.4. According to experimental results observed on various bcc/fcc metals the dependence of annihilation coefficient $R_m(T,\varepsilon`)$ [12] can be phenomenical expressed by

$$R_m \cong R_{m,o}\, (\varepsilon_{o,s}´/\varepsilon`)^{1/z} \qquad (5)$$

with the corresponding coefficient $R_{m,o}$ at T=0 K and the temperature dependent exponent $z=\mu b^3/(kTg)$ where $g \cong 0.5\text{-}1$ and $\varepsilon_{o,s}´ \approx 10^7 s^{-1}$ are empirical constants. Coefficient R_m strongly increases with increasing temperature and decreasing strain rate. Maximum strain hardening $\Delta\sigma_{\varepsilon,m}$, true fracture strain ε_f and uniform ductility ε_u, which related to the engineering strain via $\varepsilon_{u,n}$= 1– exp(-ε_u) are given by [1,7a]

$$\Delta\sigma_{\varepsilon,m}=\alpha\, \mu b M^2/(4\Lambda_o R_m)\{1+ [1+64\, R_m\, \Lambda_o^2 (b\, M)^{-1}(f_v/d_p)]^{1/2} \} \qquad (6a)$$

$$\varepsilon_f = -(1/R_m)\, \ln\{1- R_m(\sigma_{fd}/k_I - \sigma_y)/\sigma_c\} \qquad \varepsilon_u = -(1/R_m)\, \ln\{1– R_m/(1\text{-}m +R_m)[1- (\sigma_y/\sigma_c)(1\text{-}m)] \}$$

with the dislocation strength coefficient $\alpha \cong 0.1464$ [1] and the strain rate sensitivity $1 \geq m = \delta \ln\sigma_y/\delta \ln\varepsilon` = -\beta_1\, T \geq 0$ of strength. Further, strength $\sigma_c = \Delta\sigma_{\varepsilon,m}\, R_m$ defines the critical yield strength

$$\sigma_c^* = \Delta\sigma_{\varepsilon,m}\, R_m /(1 – m) = \sigma_c /(1\text{-} m) \qquad (6b)$$

above which uniform strain in tensile tests disappears ($\varepsilon_u = 0$) due to macroscopic plastic instability according to Hart`s instability concept [14] $\delta\sigma_\varepsilon(\varepsilon)/\delta\varepsilon=\sigma_\varepsilon(\varepsilon)[1-m]$, which becomes identical with Considere`s law for m=0. Deduced relations in eq. 6a take into account an enhanced dislocation multiplication (q=1) with increasing density of stored dislocations $A\propto 1/\Lambda\propto\rho^{1/2}$ because they act as strong barriers reducing mean glide distance of moving dislocations according to $\Lambda=\Lambda_o/(b\rho^{1/2})$ with the structural constant $\Lambda_o\geq b$ [1,7a]. The important critical strength σ_c* corresponds to the maximum attainable ultimate tensile strength for rate sensible metals m≥0 due to macroscopic plastic instability appearance in tensile tests for the case of condition q=1 and uniform plastic deformation. It strongly increases with increasing dispersion hardening and also weaker with increasing shear modulus. As eq. 6a demonstrates, increasing strengthening by solid solution and grain refinement reduces uniform ductility and more pronounced the fracture strain. Dispersion hardening otherwise reduces again fracture strain but increases uniform ductility due to enhanced dislocation multiplication [1] below achieve of a critical yield strength $\sigma_y=\sigma_L$. For bcc metals at very low temperatures $<0.3T_m$ (melting temperature), where glide is mainly controlled by the more heavier movable screw dislocations, their glide distance becomes mainly bounded by the grain size $\Lambda=c\ d_K$, $c\leq 1$ corresponding to constant dislocation multiplication (q=0) because they can easily around sessile dislocations by cross-slip. At higher temperatures edge dislocations then becomes easier movable and can more stronger contribute to dislocation glide. Sessile dislocations act now as strong glide barriers which reduce mean glide distance according to the considered behaviour q=1. The critical strength σ_L above which uniform strain finally becomes limited by the pronounced strength-induced reduction of fracture strain (i.e. $\varepsilon_f \leq \varepsilon_u$) in the case of q=1 can be exactly expressed by

$$\sigma_L = [(1 - m + R_m)\ (\sigma_{f,d}/k_L) - \sigma_c\ ] /\ R_m \qquad (7)$$

where k_L describes stress intensity at σ_L and $\sigma_{f,d}$ the ductile fracture stress. It demonstrates, that such limitation of uniform strain by the drop of fracture strain ε_f giving $\sigma_L \leq (\sigma_{f,d}/k_L)$ only appears if critical strength σ_c* for uniform ductility appearance becomes larger than the fracture stress $\sigma_{f,d}/k_L$. For valid of that condition, strength $\sigma_L \leq (\sigma_{f,d}/k_L)$ reduces with increasing strain rate sensitivity m and strength σ_c as given for dispersion-hardened metals, but increases with increasing annihilation coefficient R_m and finally asymptotes to $\sigma_L = (\sigma_{f,d}/k_L)$ for $R_m \rightarrow \infty$.

For the reduction of area to fracture, which related to the true fracture strain by $Z=\Delta A/A_o = 1 - \exp(-\varepsilon_f)$ it results $Z=1-\{1- R_m(\sigma_{f,d}/k_I - \sigma_y)/\ \sigma_c\ \}^{1/\ Rm}$ from eq. 6a in the case of q=1, whereby always $k_I > 1$ yields for $\sigma_y<\sigma_{f,d}$ because of $\varepsilon_u<\varepsilon_f$. For the to zero extrapolated strength $\sigma_y\rightarrow 0$ like the maximum true uniform strain $\varepsilon_{u,o}^{*}=(1/R_m)\ \ln\{1+R_m/(1-m)\}$ again their maximum arises here described by $Z_o=1 -\{1- R_m(\sigma_{f,d}/k_I)/\sigma_c\}^{1/\ Rm} \leq 1$. It reduces to the simple relation $Z_o=(R_m\ \sigma_{f,d}/k_I)/\sigma_c$ for the low annihilation coefficient $R_m=1$ as might applicably at low deformation temperatures. For that case $R_m=1$ additionally fracture strain according to $Z=(\sigma_{f,d}/k_I - \sigma_y)/\sigma_c$ reduces linearly with increasing yield strength, more stronger for dispersion-hardened metals with higher μ. It further demonstrates that for q=1 compared to constant dislocation multiplication q=0 a weaker drop of fracture strain ε_f, Z arises with increasing yield strength and maximum work-hardening $\Delta\sigma_{\varepsilon,m}$ due to fine dispersions in contrast to the behaviour of uniform ductility. For q=0 it results $\sigma_c\rightarrow\infty$ and uniform strain with the compared to q=1 initial lower maximum of $\varepsilon_{u,o}^{*}=[1/(2R_m)]\ \ln\{1+R_m/(1-m)\}$ at $\sigma_y=0$ continuously reduces with increasing yield strength and asymptotes finally to $\varepsilon_u\rightarrow\infty$ at $\sigma_y\rightarrow\infty$. Thus, bcc metals at lower T following the behaviour q=0 show higher uniform ductilities at high yield strengths but lower uniform strains at low strengths especially at $\sigma_y=0$ of their appeared maximum.

For the description of grain refinement and irradiation hardening effects on the change of the ductile impact energy shift $U=\Delta USE_{dk,i}/USE_p$ normalized to initial value of dispersion-hardened state $f_v>0$ again eq.4 can be used by replacing $\Delta\sigma_p$ through the caused strength increase $\Delta\sigma_{dk}$ or (eq. 1b) $\Delta\sigma_i$. In the case of grain refinement also an increase of fracture strength according to the Hall-Petch type relation

$$\sigma_{fd} = \sigma_{fd,o} + k_f / d_K^{1/2} \qquad (9)$$

has been additionally taken into account with the fracture stress coefficient k_f and the fracture stress $\sigma_{fd,o}$ at $d_K\rightarrow\infty$. With this, the true fracture strain then can be expressed by

$$\varepsilon_f = -(1/R_m)\ \ln\{1- [\sigma_{fd,o}/k_I - \sigma_o+(k_f - k_{HP})/d_k^{1/2}]\ R_m/\sigma_c\} \qquad (10)$$

Accordingly, the strength-induced drop of fracture strain distinctly weakens with increasing constant k_f of fracture stress increase. For the strength dependence of stress intensity at position of micro-crack nucleation the limitation $2.6\geq k_I\geq 1.8$ with a linear relation $k_I=k_{Io}-c(\sigma_y - B)$ with B=147 MPa for Ta and B=500 MPa for Ta-(20-40)W and W as well as $c=1.5\ 10^{-3}$ MPa^{-1}, $k_{Io}=2.6$ has been used. The total normalized shifts in DBTT and ductile impact energy USE according to eqs. 3,4 are finally given by

$$V_o=\Delta DBTT/DBTT_o= V_p + V(1 + V_p) \qquad U_o=\Delta USE/USE_o=U_p + U(1 + U_p) \qquad (11)$$

where shifts $V=\Delta DBTT_{dk}/DBTT_p$ and $U=\Delta USE_{dk}/USE_p$ describing grain refinement effects are normalized to the absolute values $DBTT_p$, USE_p of the dispersion-hardened state $f_v>0$ at $d_K\cong 20$ μm and $DBTT_o$, USE_o are the corresponding initial values at $f_v=0$. The pure dispersion-induced shifts are denoted by $V_p =\Delta DBTT_p/DBTT_o$ and $U_p =\Delta USE_p/USE_o$ at the normal grain size $d_K\cong 20$ μm.

3. Results

3.1 Constant ductile and dynamic fracture stresses

The main physical properties as Burger`s vector b, shear modulus μ, melting temperature T_m as well as thermal conductivity λ_{th} , linear extension coefficient α_{ex} , cross section for fast ^{14}MeV neutrons and half time of decay of main radiactive isotope are given in Tab.1 for the considered refractory metals Ta, W, Ta-40W and possible alloying elements Mo, Cr, V at room temperature (RT) which compared with α-Fe. Accordingly, the more brittle W shows the highest μ, λ_{th} and lowest thermal expansion coefficient compared to the ductile metals α-Fe and Ta. Thus, alloying of Ta with W similar as by Mo and Cr enhances strength and corrosion resistance and reduces thermal stress generation as well as hydrogen embrittlement [13]. By the little lower half time of radiactive decay for W, additionally the radiation activity is reduced as particularly required for their application as structural materials in nuclear devices. This can be further reduced by an additional alloying of Mo and Cr which reduces α_{ex} and increases λ_{th} but also μ. From the model-assisted fit of the stress-strain curves including the initial strain hardening rates, the high critical strength σ_c=1761 MPa has been deduced for pure Ta [2] at RT and $\varepsilon`=10^{-4}$ s^{-1}, d_K=20 μm, σ_y=149.5 MPa which follow the multiplication behaviour q=1 with the annihilation coefficient R_m=6.5. Critical strength increases by tungsten alloying to σ_c=2670 MPa at 20at% W, whereby R_m=6.675 and σ_y=590 MPa. These critical strengths of Ta-(0-20)W are higher than these σ_c=850-950 MPa obtained for austenitic Cr/Ni stainless steels of types AISI 304/316, DIN 1.49881 [15] at T_{irr}=T=230°C from the drop of uniform ductility by irradiation strengthening due to atomic clusters and dislocation loops formation. A somewhat lower critical strength σ_c=775 MPa is also deduced

from the dependence $\varepsilon_u(\sigma_y)$ due to irradiation strengthening for the 7-9CrWVTa(RAFM) steels (0.07-0.1 wt.% C) developed as structural materials for nuclear applications as the blanket of future fusion reactors. Increasing (C+N) contents through pronounced carbide/nitride precipitations increase according to eqs.6a,b critical strength σ_c of conventional 10CrMoVNb steels to slightly higher values of $\sigma_c \cong 1150$ MPa as found in the 10CrMoVNb steel MANET-I with 0.14 wt.% C. Thus, the high critical strength values σ_c=1761-2670 MPa of Ta-(0-40)W alloys corresponding to σ_c* for m=0 might indicate that dislocation multiplication results here by reactions of mobile with stored dislocations within the matrix and partly also by grain boundaries. Fig. 1 at first shows the observed yield strength increase for various ferritic and ferritic martensitic ODS-(7-13)CrWVTa-(0.1-0.5wt.%yttria) steels produced by powder metallurgy as a function of the dispersion parameter $(f_v)^{1/2}/d_p$, which compared with the Orowan predictions using α=0.1464, M=2.733, b=0.25 nm and μ=82.3GPa [1]. The particle strengths are obtained from the difference between the measured yield strengths of ODS-steels and base materials with the same composition, produced by the melting process. Volume fraction f_v and mean particle size d_p are measured by TEM examinations or calculated from Y_2O_3- content of $f_v=1.5618\times10^{-2}\times$(wt.%yttria). As demonstrated, the measured strengths $\Delta\sigma_p \leq 970$ MPa at the particle sizes $d_p \geq 3$ nm increases with increasing ratio $(f_v)^{1/2}/d_p$ consistently with the Orowan predictions for uniform distributed particles. The deviation of measurements toward lower strengths mainly result from softening due to the ferritic-martensitic duplex structure of ODS-steels compared to fully martensitic base steels or non-uniform particle distributions. Thus, the Orowan predictions seem to be an upper limit of achievable strengthening by oxide dispersions and non-shearable precipitates. Mainly due to the higher shear moduli a stronger dispersion hardening can by observed in ODS-Ta-W alloys at higher tungsten contents above 11 at. W % compared to ODS- (7-13)Cr-RAFM steels at the same particle factors f_v, d_p and uniform distributions. It achieves with an increase of factor ~2.1 their maximum for pure ODS-W. For the low particle fraction f_v=0.00469 corresponding to 0.3wt.% Y_2O_3 for ODS-RAFM and the mean particle size d_p=12 nm, already high dispersion strengths of $\Delta\sigma_p$= 352.9 MPa - ODS-Ta-20W, $\Delta\sigma_p$= 411.03 MPa - ODS-Ta-40W and $\Delta\sigma_p$= 670.19 MPa for ODS-W are obtained compared to $\Delta\sigma_p$= 318.13 MPa for ODS-RAFM and $\Delta\sigma_p$= 267.4 MPa for ODS-Ta. Fig. 2a shows the predicted grain size dependence of engineering uniform ductility $\varepsilon_{u,n}$ vs. $d_K^{-1/2}$ for ODS-RAFM steels at RT and d_p=12 nm, which following the work-hardening behaviour q=0 as function of f_v (0 to 0.03). The following parameters have been used for calculations: k_{HP}=6641 MPa(nm)$^{1/2}$, μ=83.3 GPa, σ_{fd}=2100 MPa and coefficient R_m=6 which predicts a maximum uniform strain of $\varepsilon_{u,o,n}$*=0.150 at m=0. For the given martensitic structure with lath thickness of ~300 nm at d_K=20 nm it is assumed that parameter c≤10 decreases with decreasing grain size and achieves c=1 for $d_K \leq 10$ nm. For lower particle fractions $f_v \leq 0.05$, most pronounced at f_v=0, uniform ductility continuously increases by grain refinement and tends to saturate at the value $\varepsilon_{u,sat}$=0.116 for nc sizes $d_K \rightarrow 0$. In accordance with predictions, this saturation ductility, which for low $\varepsilon_{u,sat}$ or μ/k_{HP} values can expressed by the simpler upper limiting approximations

$$\varepsilon_{u,sat} \leq (\alpha\, \mu/\, k_{HP})^2\, b\, M^3/[4\, c(1\text{-}m)^2\,] \;\leq\; \varepsilon_{u,o}^{\,*} \qquad (12)$$

becomes independent on volume fraction f_v and solid solution hardening. It increases with increasing m and ratio $(\mu/k_{HP})^2$ but also with increasing texture factor α^2M^3. Toward higher $\varepsilon_{u,sat}$ or lower $\mu/k_{HP} \rightarrow 0$ values, this increase of saturation ductility $\varepsilon_{u,sat}$ weakens and finally approaches the maximum value $\varepsilon_{u,sat} \leq \varepsilon_{u,o}^{\,*}=(1/R_m)\, \ln\{1+R_m/(1\text{-}m)\}$ which depends besids R_m also on m. This demonstrates, that $\varepsilon_{u,sat}$, similar as the maximum ductility $\varepsilon_{u,o}^{\,*}$ now increases with decreasing annihilation coefficient R_m and weaker also with increasing m but becomes independent on ratio $(\alpha\mu/k_{HP})$. That deduced saturation ductility generally becomes valid also for bcc/fcc metals which

initial following the behaviour q=1 because dislocation multiplication at nc region becomes finally determined by the grain size (q=0). At the higher content f_v=0.02, then $\varepsilon_{u,n}$ first weakly reduces due to grain refinement and goes through a broad minimum before it also tends to increase toward $\varepsilon_{u,sat}$. Thus, with increasing fraction f_v, uniform ductility strongly increases up to $f_v \leq 0.024$ at larger d_K but decreases weakly at lower d_K. However, when a lower critical grain size $d_{K,c} \geq 90$ nm is achieved within the uf region corresponding to $\sigma_y \geq \sigma_L$, fracture strain drastically drops and limits uniform ductility by $\varepsilon_f < \varepsilon_u$. Finally, it disappears at the nc grain size $d_{K,f}$, where $\sigma_y = \sigma_{fd}$. With increasing fraction f_v and decreasing d_p, the limiting grain size $d_{K,c}$ for a uniform ductility increase increases more strongly than $d_{K,f}$. At higher particle fractions, as $f_v \geq 0.024$ in the case of d_p=12 nm, uniform ductility then becomes always limited by $\varepsilon_f < \varepsilon_u$. Fig. 2b shows the predicted grain size dependence $\varepsilon_{u,n}$ vs. $d_K^{-1/2}$ now for ODS-Ta again at RT-q=1 as function of f_v for d_p=12 nm and for different particle sizes d_p at f_v=0.00469. Additionally, the effect of an irradiation hardening of $\Delta\sigma_i$=600 MPa is indicated. The following parameters have been used for calculations: k_{HP}=7273.5 MPa(nm)$^{1/2}$, μ=61.8 GPa, c=1 with the ductile fracture stress σ_{fd}=2100 MPa. Contrary to ODS-RAFM at RT-q=0, the initial quite higher uniform ductility with the maximum $\varepsilon_{u,o}$*=0.310 for Ta and ODS-Ta shows a continuous decrease from grain refinement, more strongly at lower d_k and would disappear in the case of f_v=0 below $d_{K,c}$=123 nm up to $d_{K,f}$=39 nm. It shows a qualitative similar behaviour as predicted for ODS-RAFM steels at the higher T=300°C, where the multiplication process change from q=0 at RT to q=1 because edge dislocations mainly control deformation [1]. However, for both RAFM and Ta at f_v=0, a transition from q=1 to q=0 occurs at lower grain sizes, which about $\varepsilon_{u,min} \approx 0.1$ for Ta because glide becomes then limited by the grain size $\Lambda = c\ d_K$. By this, uniform ductility then increases again from the minimum toward to a saturation value, which with $\varepsilon_{u,sat}$ = 0.106 for ODS- Ta is somewhat higher than $\varepsilon_{u,sat}$=0.0719 of ODS-RAFM steels at 300°C. For both ODS-Ta and ODS-RAFM otherwise at higher fractions $f_v \geq 0.00469$ and lower $d_p \leq 50$ nm, no such transition q=1→q=0 appears because glide remains always limited by the high dislocation density up to fracture. With increasing fraction f_v (0 to 0.03) as shown in Fig. 2b for d_p=12 nm, uniform ductility of ODS-Ta increases also but somewhat more weakly at lower d_K within the uf region due to the combined strong increase of critical strength σ_c. However, critical grain size $d_{K,c}$ strongly increases by increasing f_v respectively dispersion hardening. With decreasing d_p as shown for f_v=0.01, ε_u is reduced more pronounced for lower $d_p \leq 5$ nm, where uniform ductility becomes finally limited by the drop of fracture strain. Irradiation hardening of $\Delta\sigma_i$=600 MPa strongly decreases ε_u and increases $d_{K,f}$. A similar behaviour ε_u vs. $d_K^{-1/2}$ as Fig. 2c demonstrates with, however, lower ductilities occurs also for the higher W containing Ta-20W alloy (f_v=0) showing a lower $\varepsilon_{u,min}$=0.085 but somewhat larger $\varepsilon_{u,sat}$=0.11 and $d_{K,f}$ compared to pure Ta. For ODS-Ta-20W with f_v=0.01 and d_p=12 nm, uniform ductility increases at $d_K \geq 100$ nm but reduces below that earlier because transition q=1 → q=0 is suppressed by their larger $d_{K,f}$ values.

As already shown for ODS-RAFM steels in ref. [1], dispersion hardening increases uniform ductility below achieve of the critical strength $\sigma_y \leq \sigma_L$. Interestingly, maximum uniform ductility increase is attained at an optimum particle size d_{ip}*, which can be analytic expressed in the case of constant multiplication q=0 as expected for bcc metals at lower temperatures by [1]

$$d_p^* = c\ d_K\ f_v \{(\sigma_o + \sigma_{dk}^*)\ c\ d_K\ f_v^{1/2}/(\beta_{OR}\ \mu\ b\ M) - 1\}^{-1} \qquad (13a)$$

where $\sigma_{dk}^* = k_{HP}\ d_K^{-1/2}$. This optimum particle size, which for ODS-RAFM steels at RT-q=0 is at nc scale d_p*=7-22 nm increases with increasing volume fraction f_v, μ and Taylor factor M but reduces with increasing strengthening by solid solution, irradiation defects and grain refinement particularly at larger constants k_{HP}. Further, d_p* remains independent on annihilation coefficient R_m

and strain rate sensitivity m whereby, however, the maximum attainable ductility increase at d_p* increases with increasing m, initial strength $\sigma_{o,m} + \Delta\sigma_i$ and coefficient k_{HP} but reduces with increasing shear modulus. Also for enhanced multiplication q=1 again such optimum particle size d_p* appears. For higher strengths this can be analytic expressed by

$$(d_p^*)_{q=1} = \beta_{OR}\,\mu\,bM\,f_v^{1/2}\{(\sigma_o+\sigma_{dk}^*)[(\sigma_o+\sigma_{dk}^*)\,64\,R_m\,(\Lambda_o/(bM))^2\,f_v^{1/2}/(\beta_{OR}\,\mu) - 2]\}^{-1} \qquad (13b)$$

with the corresponding optimum particle hardening $\Delta\sigma_p^*=2(\sigma_o+\sigma_{dk}^*)/\{(\sigma_o+\sigma_{dk}^*)^2\Omega d_p - 1\}$ and $\Omega = 64\,R_m\,(\Lambda_o)^2 / [(bM)^3(\beta_{OR}\,\mu)^2]$, which similar to eq. 12a. Compared to q=0, optimum particle size d_p* increases for q=1 little weaker with increasing f_v (about $d_p^* \sim f_v^{1/2}$) but reduces more stronger with increasing strengthening (weaker than $d_p^* \sim 1/\sigma_o^2$) as due to grain refinement or irradiation defect formation. It remains again independent on m as for q=0, but additionally becomes now dependent on R_m. Increasing annihilation coefficients R_m reduces d_p* and the corresponding optimum particle strengthening $\Delta\sigma_p^*$. For ODS-Ta by the lower strength and shear modulus slightly higher $d_p^* \geq 30$ nm values at $f_v<0.05$ arise which, however, strongly reduce with increasing W alloying. It finally asymptotes to $d_p^* \leq 6$ nm for pure ODS-W and $d_K \leq 20$ µm. Thus, increasing tungsten alloying of ODS-Ta-W metals indirectly increases uniform ductility because their optimum shifts to higher particle strengthening. Increasing particle strengthening, however, reduces σ_L of condition $\varepsilon_f < \varepsilon_u$ which might limit this increase particularly in the case of lower fracture stresses respectively brittle metals. Fig. 3 finally shows the phase diagram of grain size vs. particle size for appearance of such increase of uniform ductility by grain refinement and dispersion hardening (DIGD) in ODS-Ta and ODS-Ta-20W alloys at f_v=0.01. With decreasing particle size and increasing W content the grain refinement must be limited clear above $d_K \cong 10$ nm to achieve DIGD. As visible, the line $d_{K,c}$ for $\sigma_y=\sigma_L$ drops more stronger with decreasing particle size than $d_{K,f}$ of $\sigma_y=\sigma_{fd}$.

As shown in [12] the fracture strain of various 9-12CrMo(W)VNb steels at RT denoted by the reduction of area to fracture continuously decreases with increasing strengthening by irradiation defects. Strengthening due to fine Y_2O_3 dispersions as observed in ODS-7CrWVTa-Eurofer´97 and the ferritic ODS-20CrAlTiC steel P2000 at 300°C enhances this fracture strain drop by pronounced work-hardening particularly at lower R_m values. At the precipitation hardened Al alloy AA611 [15] at RT by their low R_m and m values due to the low stacking fault energy indeed a linear decrease of fracture strain $Z(\sigma_y)$ with increasing strengthening is observed as predicted for R_m=1 at q=1. Fracture stress with values of $\sigma_{f,d}/k_{I,f}$=375-500 MPa and also the maximum fracture strain Z_o=0.55-1 strongly depends of the ageing temperature T_a=RT-200°C. Mean ageing temperatures T_a=100-177°C with low precipitation sizes increase ductile fracture stress $\sigma_{f,d}/I_{I,f}$ but reduce Z_o to about ≈0.55, while at the highest temperature T_a=200°C indicating over ageing, the maximum Z_o=1 results. This behaviour will be determined by the superimposed effects from alloy composition and ageing treatment upon precipitation morphology parameters f_v, d_p and stain rate and strain depending work-hardening coefficients $m=\delta\ln\sigma_y/\delta\ln\varepsilon`$ and $n=\delta\ln\sigma/\delta\ln\varepsilon$ through variation of solid solution hardening. It determines $Z_o(m)$ and also the critical damaging $\sigma_{f,d}(f_v)$ by void formation at precipitates. These observations demonstrate that also in dispersion-hardened ODS-metals as ODS-RAFM steels and ODS-Ta-W alloys besides the pronounced strengthening additionally also a change in fracture stress might occur due to present fine precipitates or dispersions.

Fig.4a shows the effect of grain refinement on the DBTT of ODS-Ta alloys as predicted by eq. 2,3 in dependence of particle size d_p=4-30 nm at constant fraction f_v=0.00469 and dynamic fracture stress $\sigma_f=r_f\sigma_{fd}$ with σ_{fd}=2400 MPa and r_f=0.9. Accordingly, DBTT increases by grain refinement more pronounced within the nc region and at lower particle sizes respectively stronger dispersion hardening. This increase within the uf grain size region of $d_K \geq 100$ nm remains, however,

comparably weaker. Additionally in Fig.4b, the critical grain size $d_{k,c}$ where DBTT achieves RT is plotted for ODS-Ta and ODS-Ta-20W alloys as function of particle volume fraction at d_p=12 nm. This limiting grain size is particularly important for alloy optimisation if excellent impact properties are required at and above RT. As shown, $d_{k,c}\geq$50 nm progressively increases with increasing particle fraction and achieves the uf size of 80 nm at f_v=0.00469 for ODS-Ta. Changes of the ductile fracture stress to 2100 and 2600 MPa at f_v=0.00469 give rise to a critical grain size change of about $+\Delta d_{k,c}\cong$30 nm and $-\Delta d_{k,c}\cong$20 nm respectively. Increasing W alloying of ODS-Ta-W shifts relation $d_{k,c}(f_v)$ due to solid solution hardening to higher critical grain sizes. For ODS-Ta-20W where $d_{k,c}\geq$120 nm it achieves already about $d_{k,c}\cong$1050 nm at f_v=0.00469. The correlation between DBTT and uniform ductility of ODS-Ta as calculated by eqs.3,6a for m=0 is shown in Fig. 5a in dependence of grain refinement and dispersion hardening through variation of the particle size $4\leq d_p\leq 30$ nm at f_v=0.00469. As demonstrated, DBTT continuously increases with decreasing uniform strain in first order about along a master curve, more pronounced at lower d_p and higher DBTT values. It indicates that DBTT and uniform ductility are equivalent parameters due to their strong dependency on yield strength, which more pronounced for DBTT compared to ε_u. Thus, grain refinement reduces uniform ductility and increases distinctly DBTT more stronger at lower d_p. For particle sizes below d_p<8 nm at f_v=0.00469, the uniform ductility decrease then becomes more enhanced due to its limitation ($\varepsilon_f<\varepsilon_u$) by the strong reduction of fracture strain at high yield strengths above the critical value σ_L as also shown in Fig. 5a by the dotted line. At high DBTT and strength values this limitation shifts the dependence DBTT vs. ε_u to lower uniform ductilities. The (- . –) lines otherwise denotes the maximum achievable uniform ductility for high ductile fracture stresses without their limitation by the fracture strain (i.e. $\varepsilon_f<\varepsilon_u$). A reduction of fracture stresses at constant ratio $r_f=\sigma_f/\sigma_{fd}$=0.9 increases DBTT and reduces also strongly uniform ductility because it becomes more stronger limited by the lower fracture strain via a decrease of σ_L. Thus, the dependence DBTT(ε_u) together with their achievable maximum DBTT($\varepsilon_{u,max}$) for higher fracture stresses σ_{fd} shift to lower uniform ductilities especially at lower DBTT values. The increase in DBTT by dispersion hardening can be approximated by $V_p=\Delta DBTT_p/DBTT_o\cong 2.416\ 10^{-3}\Delta\sigma_p$. Grain refinement increases DBTT and reduces USE, thus, degradates impact properties. The effect of grain refinement on the correlation between DBTT and the ductile upper shelf energy shift $U=\Delta USE_{dk}/USE_p$ of ODS-Ta is shown in Fig. 5b as function of volume fraction f_v=0-0.03 at d_p=12 nm and r_f=0.9. Also lines for constant grain sizes are indicated in that plot. As demonstrated, a grain refinement increases initial weaker DBTT but more stronger the ductile energy reduction U. At lower grain sizes then the DBTT increase enhances and shift U asymptotes quickly to $U\rightarrow 1$ according to $USE\rightarrow 0$. Increasing particle volume fraction increases further the initial DBTT value at larger d_K and additionally enhances the grain refinement-induced increase of DBTT and shift U particularly at low grain sizes ≥0.25 μm of uf and nc regions.

3.2 Effect of a grain refinement-induced increase of ductile/dynamic fracture stresses $c_f > 0$

Fig. 6a shows the effect of a grain refinement-induced increase of fracture stresses denoted by the ratio $1.5\geq c_f=k_f/k_{HP}\geq 0$ on the correlation between DBTT and uniform ductility of ODS-Ta alloys through grain refinement at f_v=0.00469, d_p=12nm, $\sigma_{fd,o}$=2400 MPa and d_K=20 μm, ε_f=0.4. Most interestingly, a minimum in DBTT within the uf region $d_{k,min}\cong$100-200 nm results which becomes more pronounced at higher ratios $c_f\geq$0.3 respectively for a stronger fracture stress increase at constant r_f=0.9. In pure Ta that minimum appears at comparably lower grain sizes 30–70 nm within the nc region. That grain size at DBTT minimum together with its $DBTT_{min}$ value increase with pronouncing dispersion hardening. Besides, increasing ratio c_f shifts the region of boundary condition $\varepsilon_f<\varepsilon_u$ to lower grain sizes and higher DBTT values promoting an additional uniform

ductility increase. Furthermore in Fig. 6b, the critical grain sizes $d_{k,c}$ for ODS-Ta, Ta-W and ODS-Ta, ODS-Ta-20W alloys are plotted in dependence of ratio $c_f=k_f/k_{HP}$ at $f_v= 0.00469$ and $d_p=12$ nm. It progressively decreases with increasing ratio $c_f \leq 1.5$ for the Ta, Ta-20W and ODS-Ta alloys but distinctly weaker at the higher-strengthened ODS-Ta-20W. For pure Ta the obtained critical grain sizes $d_{k,c}$=3-33 nm are within the lower bond of the nc region and shift by pronounced dispersion strengthening for ODS-Ta to $d_{k,c}$=8.25-76 nm of the upper bond of nc region. As shown for Ta also the grain size $d_{K,min}$ at minimum $DBTT_{min}$ decreases weakly with increasing ratio c_f. Pronounced solid solution hardening of the Ta-20W alloy again shifts relation $d_{k,c}(f_v)$ to higher $d_{k,c} \leq 155$ nm which reaches already the uf region. At ODS-Ta-20W then a distinctly stronger increase of critical grain size to $0.8 \leq d_{k,c} \leq 17.5$ μm arises for $c_f \leq 1.5$ by additionally weakening the dependence $d_{k,c}(c_f)$. Figs. 7a,b show the effect of a grain refinement-induced increase of dynamic and ductile fracture stresses described by the ratio $c_f=k_f/k_{HP}>0$ on the correlation between DBTT and the ductile energy reduction U of ODS-Ta (a) and Ta-20W(b) alloys due to grain refinement. As indicated for ODS-Ta at f_v=0.00469, d_p=12 nm increasing c_f reduces stronger DBTT and weaker energy shift U. Besides, again a distinct minimum in DBTT of 60–120 K appears around the nc grain size of $d_{K,min} \cong 85$ nm for $c_f \geq 0.5$ which pronounces at higher c_f values by decreasing the $DBTT_{min}$ value and weaker also $d_{K,min}$. For grain sizes below $d_{K,min}$ both DBTT and shift U are strongly increased. At the Ta-20W alloy this minimum of $DBTT_{min} \geq 110$ K becomes broader and appears at sligthly larger $d_{k,min} \geq 150$ nm values (Fig.5b) than for pure Ta. Additionally, at higher ratios $c_f \geq 0.8$ and grain sizes $d_k \geq 200$ nm the ductile energy shift U becomes negative at a certain higher optimum grain size $d_{K,min} \cong$ 300 nm as for the minimum $DBTT_{min}$ corresponding to an increase of USE. Fig. 8a shows the grain size dependence of DBTT for the higher tungsten containing Ta-40W alloy at $5 \geq c_f \geq 0$. Accordingly, the DBTT increases by grain refinement from initial value 153 K for the normal grain size d_K=20 μm, more pronounced below $d_K \leq$ 400 nm of uf grain sizes. For a mean fracture stress increase with ratios $0.3 \leq c_f \leq 2$, the $DBTT_{min}$ appears at the optimum grain size of 400-500 nm and toward lower d_k, then again DBTT strongly increases. At high ratios $c_f \geq 1.5$, then DBTT continuously decreases also within the nc region while energy shift U is increased after going through its minimum. This demonstrates Fig.8b where the map of relative shifts $V_o=\Delta DBTT_{dk}/DBTT_o$ vs. $U_o=\Delta USE_{dk}/USE_o$ is shown in dependence of grain refinement for various c_f=0.5 to 5 values. At lower $c_f \leq 1$, maximum reductions of V_o and U_o are achieved by grain refinement at somewhat higher $d_{k,min} \geq 600$ nm. Toward the nc regime shifts V_o and U_o strongly increase where fracture becomes strain controlled at achieve of the critical strain ε_f=0.4. The behaviour V vs. $U_p=\Delta USE_{dk}/USE_p$ for ODS-Ta-40W is shown in Fig. 9 for f_v=0.001, d_p= 12 nm. For low $c_f \leq 1.5$, the initial higher V_p=0.247 and $U_p > 0$ values of dispersion-strengthened ODS-Ta-40W compared to the base alloy Ta-40W continuously increase further by grain refinement. At the higher c_f=2.5 value then shift V decreases up to the nc region while U_p becomes negative corresponding to a decrease of impact energy USE and goes through a sharp minimum around $d_{K,min}$=100 nm after which it again increases. It becomes then positive at the nc region while shift V still further reduces due to decrease of DBTT. Thus, increasing tungsten alloying of ODS-Ta-W restricts the applicable grain refinement if only a weak fracture stress increase occur and if low DBTT≤RT values are required but additionally enhances strength and more stronger their hydrogen embrittlement resistance. Finally Fig. 10 shows the predicted grain refinement effects of pure tungsten at RT in dependence of ratio $1.5 \leq c_f \leq 5$ of fracture stress increase which compared with experimental results reported by [4]. Following parameters have been used for predictions: R_m=4.5, k_{HP}=7273.24 MPa(nm)$^{1/2}$, μ=160 GPa, σ_y=725 MPa, r_f=0.9, $\beta_o=5.35\ 10^{-3}\ K^{-1}$, $\beta_1= -1.09\ 10^{-4}\ K^{-1}$, P=1125 MPa, as well as σ_c=2670 MPa, $\sigma_{fd,o}$=1600 MPa and R_m=4.5. It predicts a maximum attainable uniform ductility of $\varepsilon_{u,on}$*=0.315 which, however, due to the low fracture stress generally limited by $\varepsilon_f < \varepsilon_u$. The measured DBTT values strongly drops from ~542 K at d_K=120 μm to ~300 K at the uf grain size of d_K=1000 nm. Toward higher

grain sizes 1000 >d_K>120 μm again DBTT decreases to ~450 K. At the mean ratio c_f=1.5, the model predicts a minimum of $DBTT_{min}$ ≅ 400 K at $d_{K,min}$= 100 nm below which it strongly increases. At higher ratios c_f=2.5/ 5, the grain refinement, however, continuously reduces DBTT. If then fracture stress below d_K= 500 nm remains constant, the DBTT would again strongly increase as denoted by the -.- dotted lines. The measured drop in DBTT agree about with predictions for an initial strong fracture stress increase via the ratio c_f=5 up to about d_K= 1000 nm. The measured DBTT reduction otherwise at high grain sizes above d_K≅ 120 μm results due to softening by recrystallization of about $\Delta\sigma_o$≅ 98 MPa. By grain refinement of the carbide (TiC, Mo_2C) dispersed W-0.3TiC-1.7Mo alloy [17] produced by mechanical alloying following sintering and hot working again such strong increase of fracture stress up to about σ_f≅2400 MPa at d_K=500-1150 nm have been observed with TiC, Mo_2C precipitates of nc sizes 10-25 nm. Thus, grain refinement particularly to the uf region of 100-1000 nm offers the possibility for ductilisation of usual brittle metals such as W, Cr, Mo and strong dispersion-hardened ODS-RAFM and ODS-Ta-W alloys by a possibly resulting strong increase of fracture stresses due to change of fracture process.

4. Conclusions and summary

The following can summarize the main results of this work:
A strong dispersion hardening via the Orowan process increases uniform ductility of ODS-Ta-W alloys like generally of bcc and fcc metals whereas it is reduced by solid solution, grain boundary and irradiation strengthening. Such paradocs behaviour of enhanced ductility by increasing strengthening has been observed in ferritic-martensitic ODS-(7-13)Cr steels [1] and uf grained AL [18] produced by ECAP. The uniform ductility maximum is achieved at a nano-scaled optimum particle size d_p* which reduces with increasing matrix strength, grain refinement and shear modulus as well as decreasing particle fraction but remains independent of strain rate sensitivity m of strength. For martensitic ODS-(7-13)CrW(Mo)VTa(Nb) steels the optimum particle size achieves d_p*=7-22 nm at RT for f_v<0.05. For pure ODS-Ta a certain larger optimum particle size d_p*≅30-40 nm arises which strongly reduce with increasing W alloying and achieves finally d_p*≤ 5 nm for pure ODS-W at d_K≤ 20 μm. In ODS-W alloys a larger uniform ductility increase might be achieved particularly in the case of a strong dispersion strengthening which, however, becomes limited by the usual lower fractures stresses in these materials which easily leads to appearance of condition $\sigma_y < \sigma_L$ already at larger grain sizes. Grain refinement to the uf scale as observed in pure W increases dynamic and ductile fracture stresses and, thus, increases uniform ductility and reduces DBTT. It is also expected that such increase of fracture stresses might occur in Ta-W alloys which would additionally enhance their ductility. For Ta-W alloys at lower W contents the larger optimum particle sizes <40 nm might be achieved also by precipitation reactions from usual fabrication process by the melting reducing production costs.
Grain refinement of Ta-W alloys increases DBTT and reduces upper shelf energy USE as well as uniform ductility in the case of constant ductile/dynamic fracture stresses. By their dominant strength dependences both DBTT and uniform ductility correlate, whereby DBTT always strongly increases with a reduction of uniform ductility either by grain refinement or solid solution strengthening and cold working. Dispersion hardening of ODS-Ta-W alloys increases further DBTT and reduces USE. At a very high total strength, especially of a strong dispersion strengthening additionally now uniform ductility might be strongly reduce particularly at lower ductile fracture stresses and grain sizes by their limitation due to the pronounced drop of fracture strain (i.e. $\varepsilon_f < \varepsilon_u$) at $\sigma_y<\sigma_L$.
A combined strong increase of dynamic/ductile fracture stresses by grain refinement denoted by the ratio $c_f = k_f/k_{HP}$ at r_f=const., however, firstly reduces strongly DBTT and weaker also impact energy shift U of (ODS)-Ta-W alloys. Minima in $DBTT_{min}$ and energy shift U_{min} result at different

optimum grain sizes already at mean ratios $c_f \geq 0.3$ of fracture stress increases. Toward nc sizes again DBTT and shift U are increased. These optimum grain sizes which for Ta, ODS-Ta are within the uf region of $d_{k,min} \cong 50–200$ nm increase with increasing W content. Besides, also the critical grain size d_{kc}, where DBTT achieves RT is increased by increasing W content, more pronounced for ODS-(20-40)W alloys at low ratios c_f. It restricts the suitable amount of grain refinement and dispersion hardening for their low temperature application if DBTT<RT is required. Dependent on grain size and dispersion hardening and fracture stress increase ratio c_f the optimum W content of ductile ODS-Ta-W alloys for their high temperature application are between 20 to ≤40at% W, where indeed hydrogen embrittlement already disappear [13] by an additional increase of corrosion resistance. A higher W content within this region in combination with a medium dispersion hardening is favourable for nuclear application up to <1300°C where sufficient RT-ductility is required. Grain refinement with a combined increase of fracture stresses can further strongly improve embrittlement resistance of these alloys as found in uf grained W alloys and additionally increases uniform ductility by an increase of fracture strain with more stronger suppress of appearance of condition $\varepsilon_f < \varepsilon_u$ at $\sigma_y < \sigma_L$.

References

[1] D. Preininger, J. Nucl. Mater. 329-333 (2004), p.362.
[2] D.H. Lassilla, A. Goldberg, R. Becker, Metall. and Mater. Transaction 33A (2002), p.3457.
[3] K.T. Hartwig, S.N. Mathandhu, H.J. Maier and I. Karaman, Ultrafine Grained Materials II (EDs.: Y.T. Zhu et al., TMS (The Minerals Metals&Materials Society), (2002), p.151-160.
[4] S.W.H. Yih, C.T.W. (1979), Tungsten: sources, metallurgy, properties and application, N.Y. and London, Plenum Press.
[5] T.G. Nieh, J. Wadsworth, Scr. Metall. Mater. 27 (1992), p.1195.
[6] F.J. Zerilli and R.W. Armstrong, J. Appl. Phys. 68 (1990), p.1580.
[7] D. Preininger, 15. Sym. Verbundwerkstoffe, 6-8.April 2004, Kassel, Proc. ED. M Schlimmer, DGM, ISBN 3-88355-340.9, p. 93-99(a) and p. 277-283(b).
[8] K.G. Hoge and A.K. Mukherjee, J. Mater. Sci. 12 (1977), p.1666.
[9] T. Suzuki, H. Koizumi and H.O.K. Kirchner, Acta Met. 43 (1995), p.2177.
[10] G.R. Odette, T. Yamamoto, H.J. Rathbun, M.Y. He et al., J. Nucl. Mater. 323 (2003), p.313.
[11] M. Shimojo, R. Jguchi, T.H. Myeong and Y. Higo, Metall and Transaction 28A (1977), p.1341.
[12] D. Preininger, J. Nucl. Mater. 307-311 (2002), p.514.
[13] A. Luo, D. L. Jacobson, K.S. Shin, Refrac. Metals 10 (1991), p.107.
[14] E.W. Hart, Acta metall. 15 (1967), p.351.
[15] D. Preininger, Proc. Stainless Steels`96, June 3-5 (1996), ISDN 3-514-00601-6 (VDEh) p.295.
[16] D. J. Lloyd, Scripta Materialia 48 (2003), p.341.
[17] Y. Ishijima, H. Kurishita, M. Hasagawa, J. Nucl. Mater. 329-333 (2004), p.775.
[18] H. W. Höpple, J. May and M. Göken, Advanced Eng. Materials, 6 (2004), p.781.

List of figures

Fig.1: Comparison of observed particle strengthening $\Delta\sigma_p$ of various ODS-(7-13)Cr steels with Orowan predictions in dependence of $(f_v)^{1/2}/d_p$. The indicated references are given in [1].

Fig. 2a: Predicted grain size dependence $\varepsilon_{u,n}$ vs. $d_K^{-1/2}$ for ODS-RAFM steels at RT-q=0 and d_p=12 nm as function of f_v.

Fig. 2b: Predicted grain size dependence $\varepsilon_{u,n}$ vs. $d_K^{-1/2}$ for ODS-Ta at RT-q=1 and d_p=12 nm as function of f_v.

Fig. 2c: Predicted grain size dependence $\varepsilon_{u,n}$ vs. $d_K^{-1/2}$ for ODS-Ta-20W at RT-q=1 and d_p=12 nm as function of f_v.

Fig. 3: Phase diagram of d_K vs. d_p for appearance of an increase of uniform ductility by grain refinement and dispersion hardening (DIGD) in ODS-(0-20)Ta alloys at f_v=0.01.

Fig. 4a: Effect of grain refinement on the DBTT increase of ODS-Ta in dependence of particle size d_p= 4-30 nm for f_v=0.00469.

Fig. 4b: Critical grain size $d_{k,c}$ (where DBTT=300 K) for ODS-Ta and ODS-Ta-20W as function of particle fraction f_v at d_p=12 nm.

Fig. 5a: Correlation DBTT vs. uniform ductility of ODS-Ta in dependence of grain refinement and dispersion hardening by variation of particle size $4 \leq d_p \leq 30$ nm at f_v=0.00469.

Fig. 5b: Effect of grain refinement on the correlation between DBTT and impact energy shift U of ODS-Ta as function of f_v= 0-0.03 at d_p=12 nm and. Lines for constant d_K are indicated.

Fig. 6a: Effect of ratio $c_f=k_f/k_{HP}$ on the correlation between DBTT and uniform ductility of ODS-Ta alloys due to grain refinement at d_p=12 nm.

Fig. 6b: Critical grain size $d_{k,c}$ where DBTT=RT for Ta, Ta-20W and ODS-Ta, ODS-Ta-20W alloys in dependence of ratio $c_f=k_f/k_{HP}$ at f_v= 0.00469, d_p=12 nm.

Fig. 7a,b: Effect of ratio $c_f=k_f/k_{HP}$ on the correlation between DBTT and ductile impact energy reduction U of ODS-Ta (a) and Ta-20W (b) alloys due to grain refinement.

Fig. 8a: Effect of ratio $5 \geq c_f=k_f/k_{HP} \geq 0$ of fracture stress increase on the grain size dependence of DBTT for Ta-40W.

Fig. 8b: Effect of ratio $5 \geq c_f=k_f/k_{HP} \geq 0$ of fracture stress increase on the grain size dependence of the shifts V_o vs. U_o for Ta-40W.

Fig. 9: Effect of ratio $2.5 \geq c_f=k_f/k_{HP} \geq 0$ of fracture stress increase on the grain size dependence of the shifts V_o vs. U_p for ODS-Ta-40W at f_v=0.001, d_p=12nm.

Fig. 10: Comparison of measured grain size dependence of pure tungsten with predictions - Effect of the fracture stress increase ratio $5 \geq c_f=k_f/k_{HP} \geq 0$.

Tables

Tab. 1: Main physical properties of Ta, W, Ta-40at% W and Mo, Cr which compared with α-Fe.
(d.. days, h.. hours, Θ..cross section for ^{14}MeV neutrons)

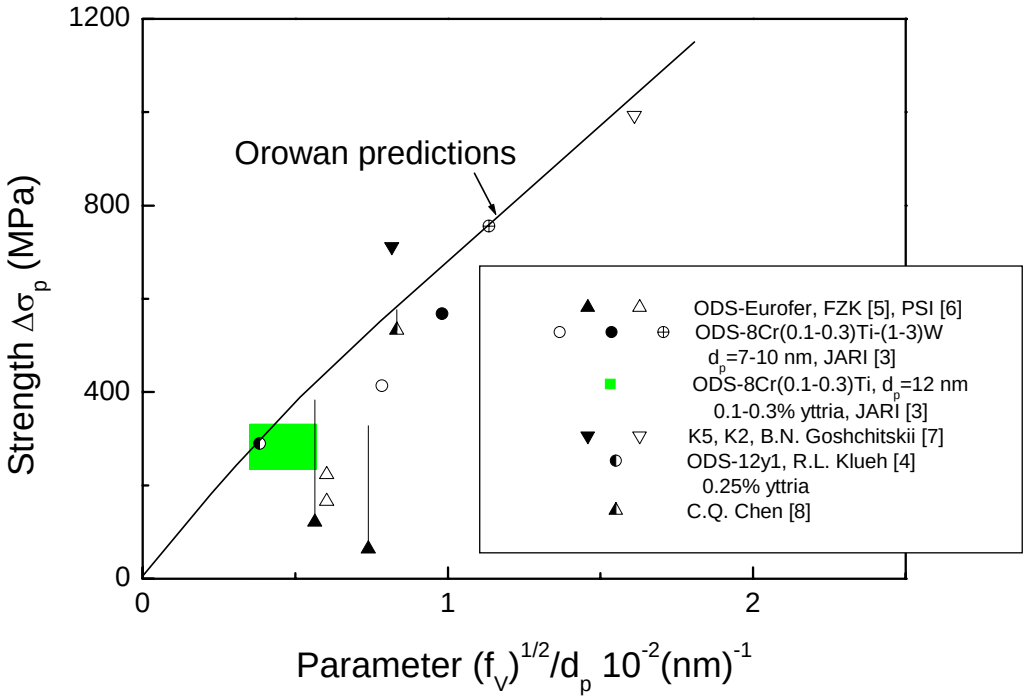
1200
800
400
0
0
1
2
Strength $\Delta\sigma_p$ (MPa)
Parameter $(f_V)^{1/2}/d_p\ 10^{-2}(nm)^{-1}$
Orowan predictions
ODS-Eurofer, FZK [5], PSI [6]
ODS-8Cr(0.1-0.3)Ti-(1-3)W
d_p=7-10 nm, JARI [3]
ODS-8Cr(0.1-0.3)Ti, d_p=12 nm
0.1-0.3% yttria, JARI [3]
K5, K2, B.N. Goshchitskii [7]
ODS-12y1, R.L. Klueh [4]
0.25% yttria
C.Q. Chen [8]

Fig. 1

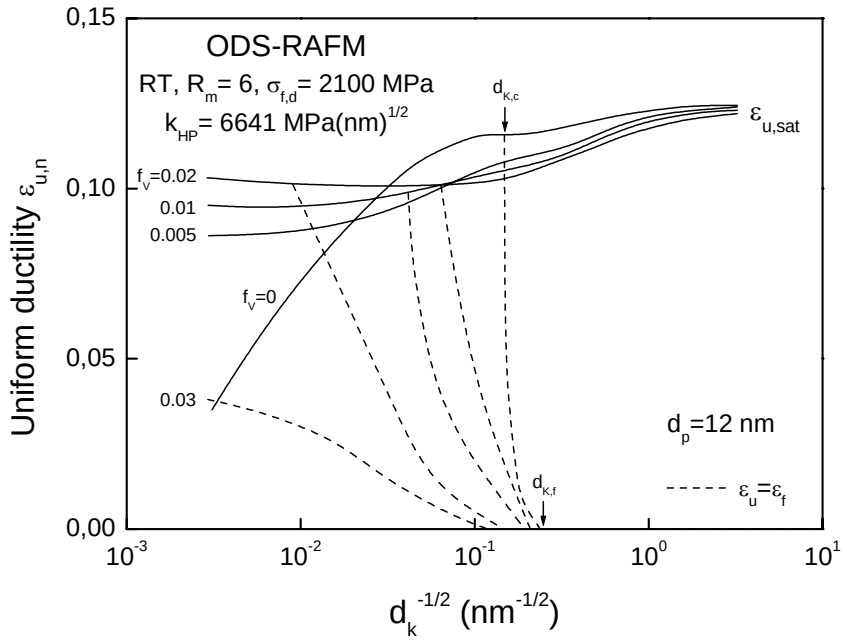
ODS-RAFM
RT, R_m= 6, $\sigma_{f,d}$= 2100 MPa
k_{HP}= 6641 MPa(nm)$^{1/2}$
$d_{K,c}$
$\varepsilon_{u,sat}$
f_V=0.02
0.01
0.005
f_V=0
0.03
$d_{K,f}$
d_p=12 nm
ε_u=ε_f
Uniform ductility $\varepsilon_{u,n}$
0,15
0,10
0,05
0,00
10^{-3}
10^{-2}
10^{-1}
10^{0}
10^{1}
$d_k^{-1/2}$ ($nm^{-1/2}$)

Fig. 2a

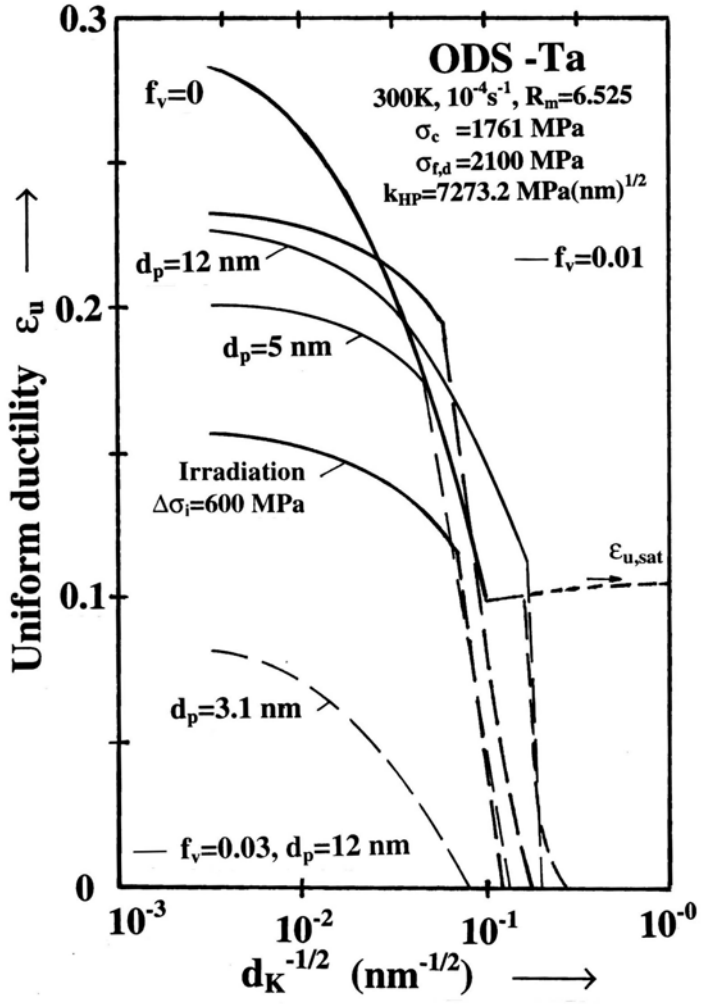
ODS -Ta
300K, 10⁻⁴s⁻¹, Rm=6.525
σc =1761 MPa
σf,d =2100 MPa
kHP=7273.2 MPa(nm)^1/2
fv=0
— fv=0.01
dp=12 nm
dp=5 nm
Irradiation
Δσi=600 MPa
εu,sat
dp=3.1 nm
— fv=0.03, dp=12 nm
Uniform ductility εu
dK^-1/2 (nm^-1/2)
0.3
0.2
0.1
0
10^-3
10^-2
10^-1
10^-0

Fig. 2b

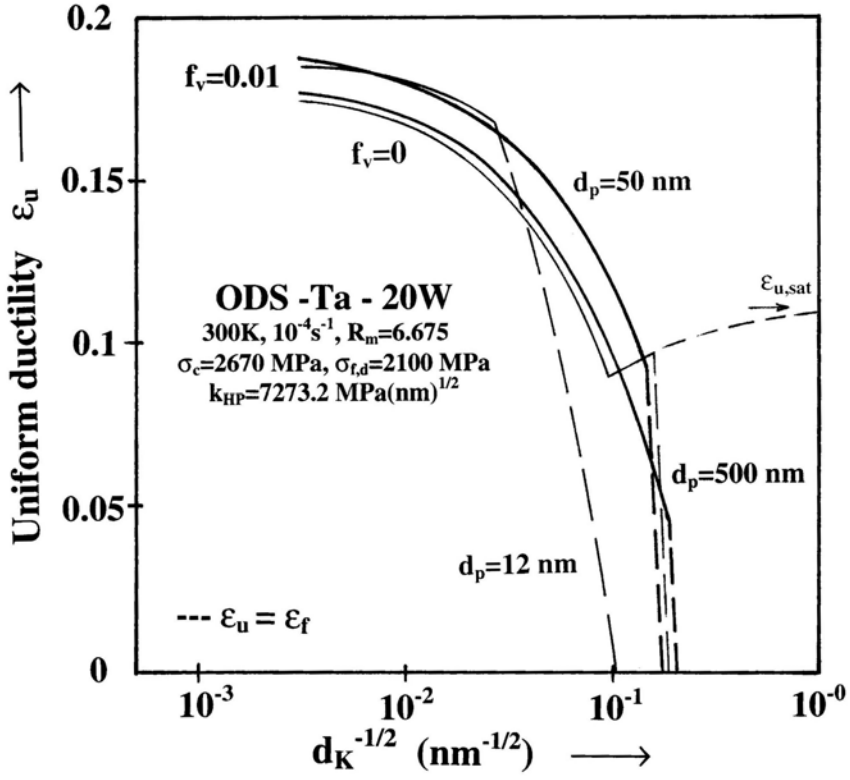
fv=0.01
fv=0
dp=50 nm
εu,sat
ODS -Ta - 20W
300K, 10⁻⁴s⁻¹, Rm=6.675
σc=2670 MPa, σf,d=2100 MPa
kHP=7273.2 MPa(nm)^1/2
dp=500 nm
dp=12 nm
--- εu = εf
Uniform ductility εu
dK^-1/2 (nm^-1/2)
0.2
0.15
0.1
0.05
0
10^-3
10^-2
10^-1
10^-0

Fig. 2c

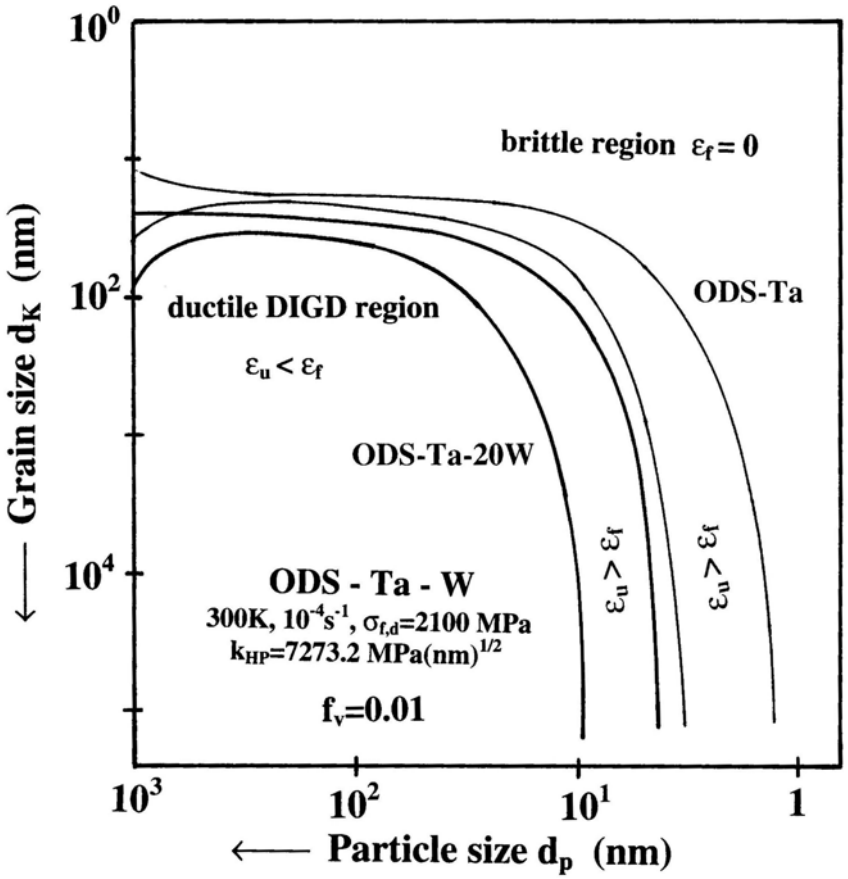
brittle region $\varepsilon_f = 0$
ODS-Ta
ductile DIGD region
$\varepsilon_u < \varepsilon_f$
ODS-Ta-20W
ODS - Ta - W
300K, $10^{-4}s^{-1}$, $\sigma_{f,d}$=2100 MPa
k_{HP}=7273.2 MPa(nm)$^{1/2}$
f_v=0.01
$\varepsilon_u > \varepsilon_f$
$\varepsilon_u > \varepsilon_f$
Grain size d_K (nm)
Particle size d_p (nm)

Fig. 3

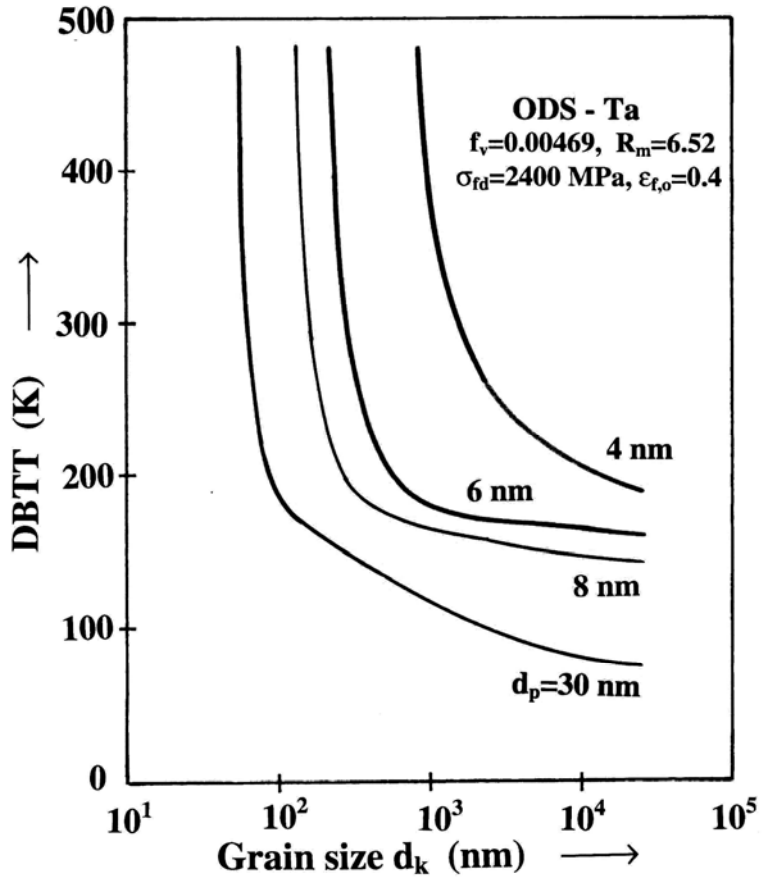
ODS - Ta
f_v=0.00469, R_m=6.52
σ_{fd}=2400 MPa, $\varepsilon_{f,o}$=0.4
4 nm
6 nm
8 nm
d_p=30 nm
DBTT (K)
Grain size d_k (nm)

Fig. 4a

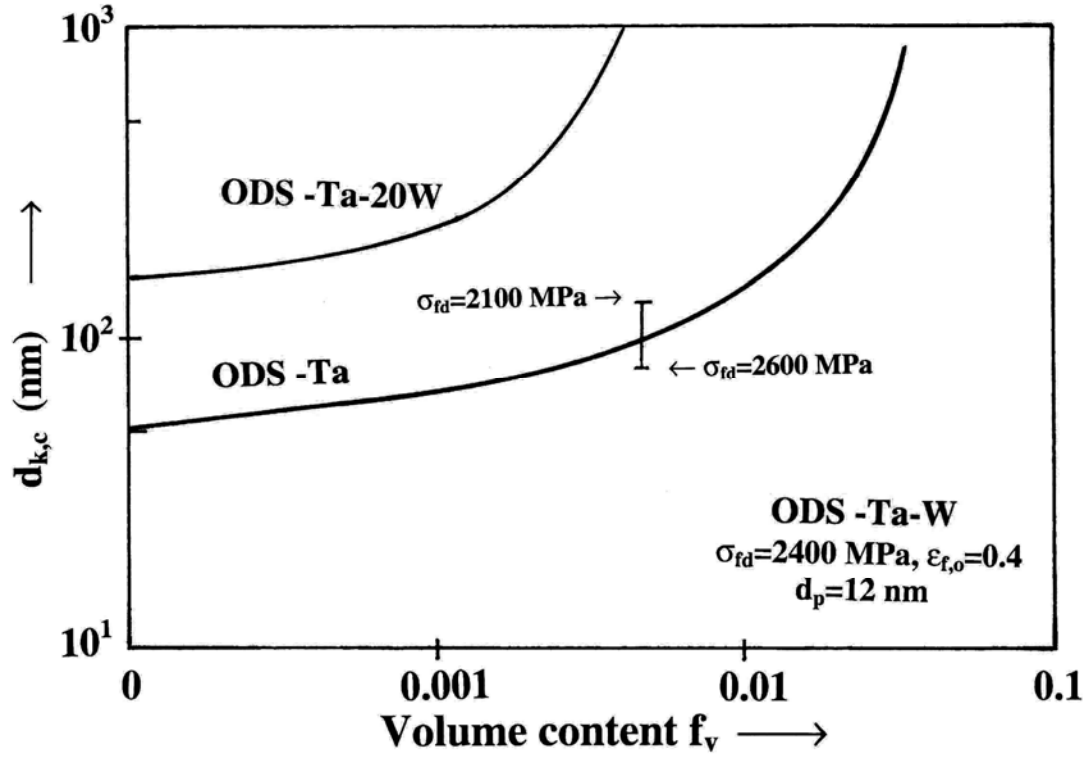
10^3
10^2
10^1
$d_{k,c}$ (nm) ⟶
ODS -Ta-20W
σ_{fd}=2100 MPa →
← σ_{fd}=2600 MPa
ODS -Ta
ODS -Ta-W
σ_{fd}=2400 MPa, $\varepsilon_{f,o}$=0.4
d_p=12 nm
0
0.001
0.01
0.1
Volume content f_v ⟶

Fig. 4b

Fig. 5a

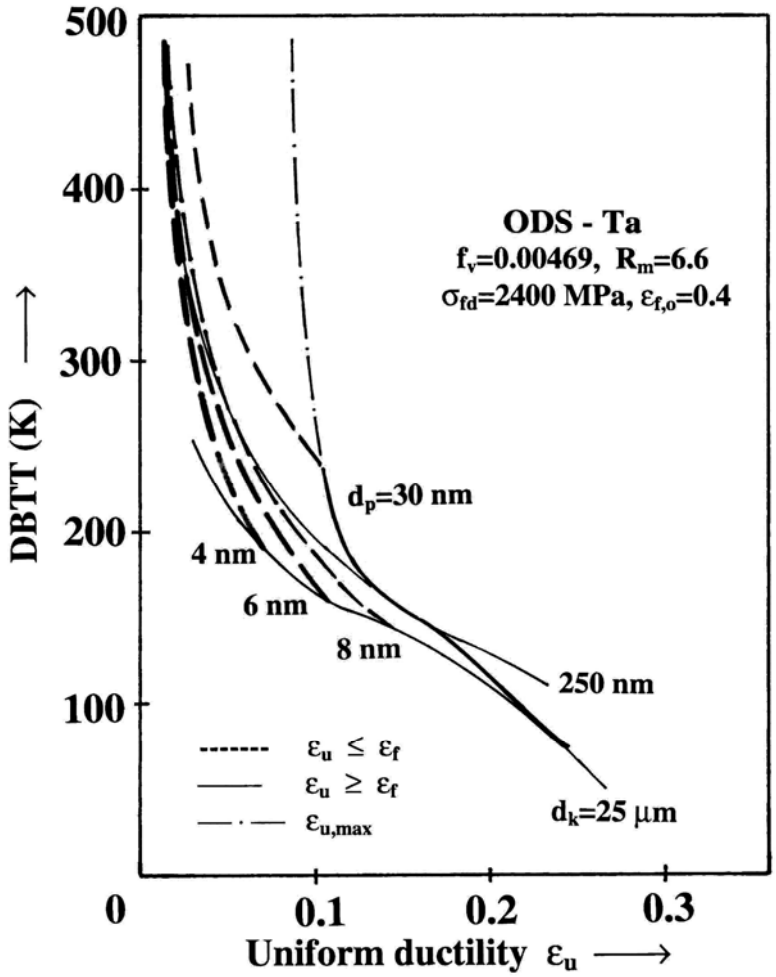
ODS - Ta
f_v=0.00469, R_m=6.6
σ_{fd}=2400 MPa, $\varepsilon_{f,o}$=0.4
d_p=30 nm
4 nm
6 nm
8 nm
250 nm
d_k=25 μm
$\varepsilon_u \leq \varepsilon_f$
$\varepsilon_u \geq \varepsilon_f$
$\varepsilon_{u,max}$
DBTT (K) ⟶
Uniform ductility ε_u ⟶
500
400
300
200
100
0
0.1
0.2
0.3

Fig. 5b

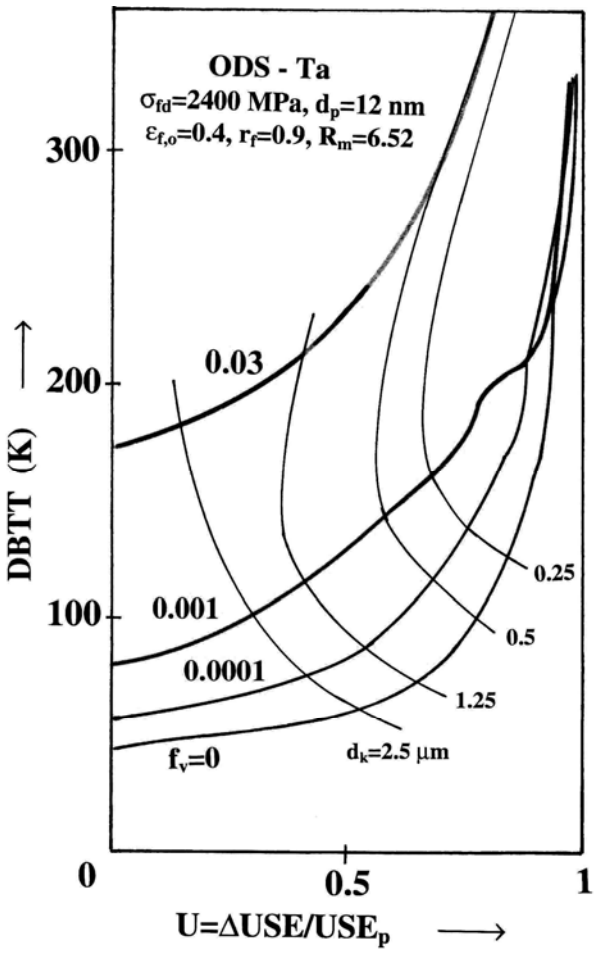
ODS - Ta
σ_{fd}=2400 MPa, d_p=12 nm
$\varepsilon_{f,o}$=0.4, r_f=0.9, R_m=6.52
0.03
0.001
0.0001
f_v=0
d_k=2.5 μm
0.25
0.5
1.25
DBTT (K) ⟶
U=ΔUSE/USE$_p$ ⟶
300
200
100
0
0.5
1

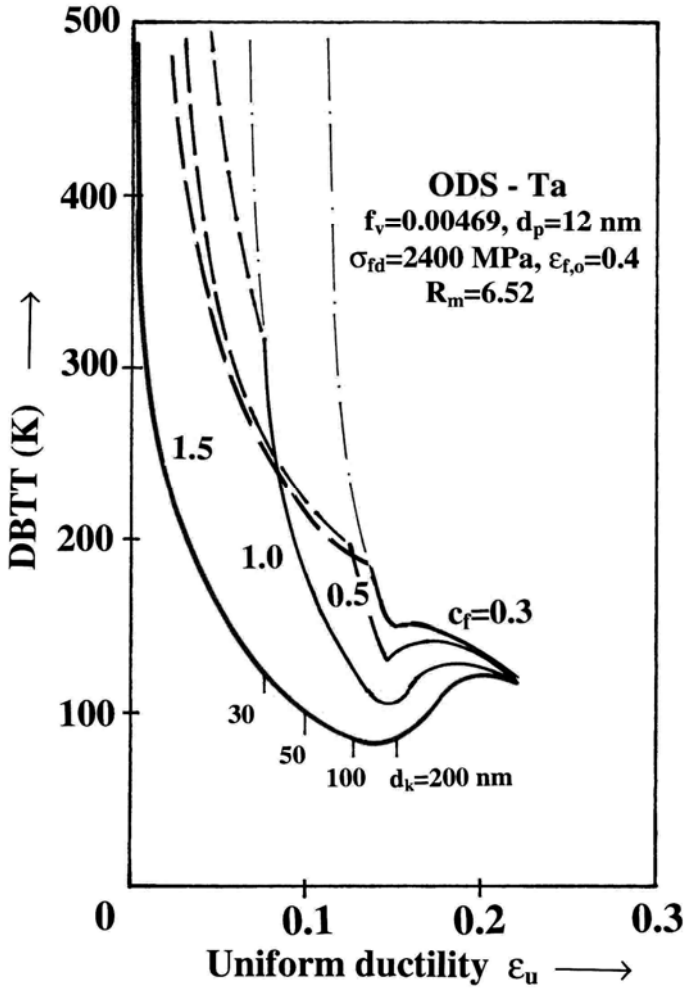
ODS - Ta
f_v=0.00469, d_p=12 nm
σ_{fd}=2400 MPa, $\varepsilon_{f,o}$=0.4
R_m=6.52
DBTT (K) ⟶
1.5
1.0
0.5
c_f=0.3
30
50
100
d_k=200 nm
500
400
300
200
100
0
0.1
0.2
0.3
Uniform ductility ε_u ⟶

Fig. 6a

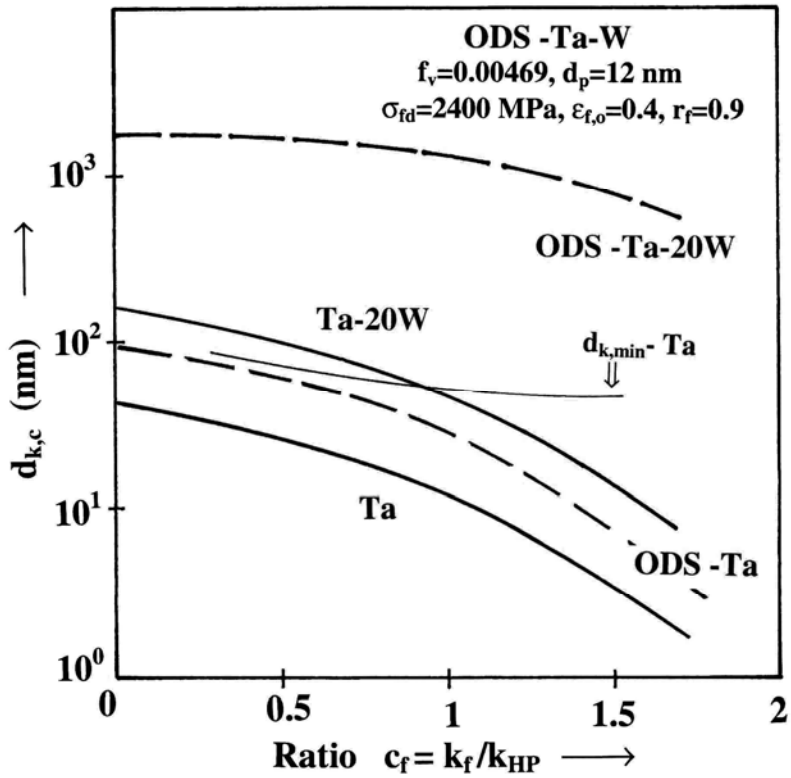
ODS -Ta-W
f_v=0.00469, d_p=12 nm
σ_{fd}=2400 MPa, $\varepsilon_{f,o}$=0.4, r_f=0.9
ODS -Ta-20W
Ta-20W
$d_{k,min}$- Ta
Ta
ODS -Ta
$d_{k,c}$ (nm) ⟶
10^3
10^2
10^1
10^0
0
0.5
1
1.5
2
Ratio $c_f = k_f/k_{HP}$ ⟶

Fig. 6b

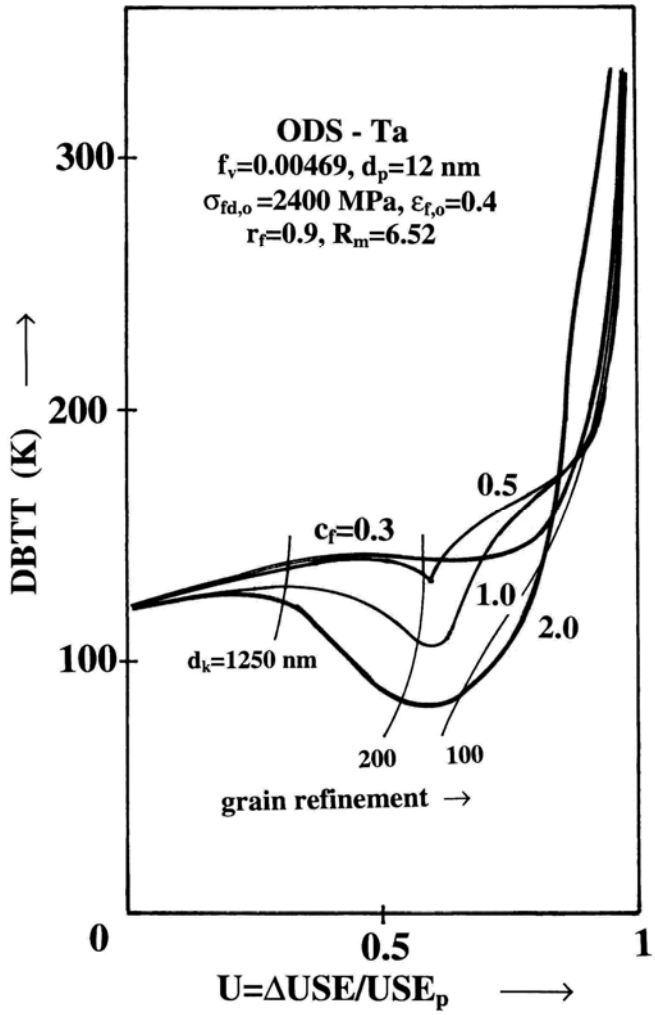
ODS - Ta
f_v=0.00469, d_p=12 nm
$\sigma_{fd,o}$=2400 MPa, $\varepsilon_{f,o}$=0.4
r_f=0.9, R_m=6.52
DBTT (K) ⟶
300
200
100
0
0.5
1
0.5
c_f=0.3
1.0
2.0
d_k=1250 nm
200
100
grain refinement →
U=ΔUSE/USE$_p$ ⟶

Fig. 7a

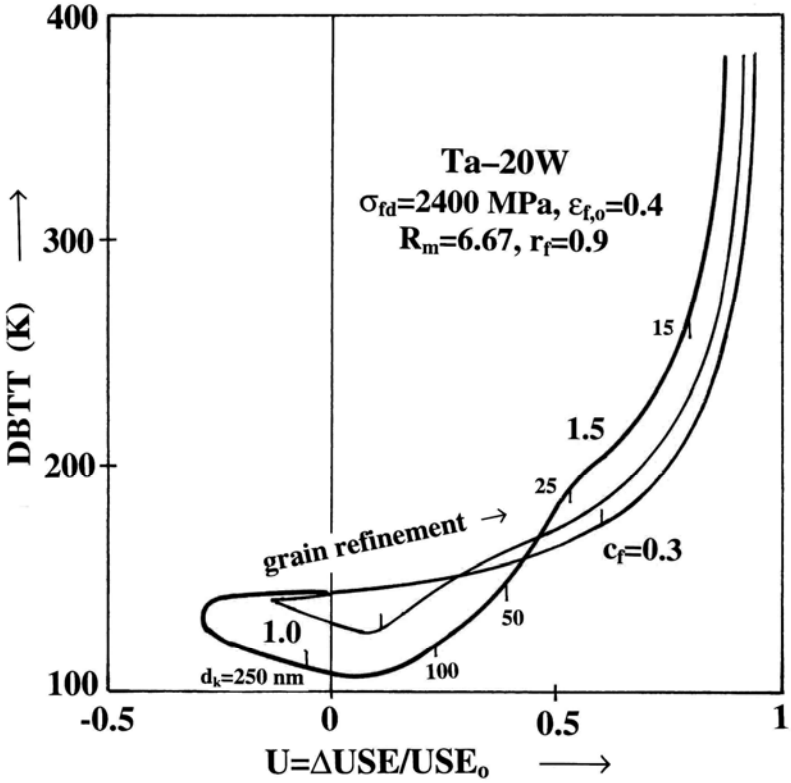
Ta–20W
σ_{fd}=2400 MPa, $\varepsilon_{f,o}$=0.4
R_m=6.67, r_f=0.9
DBTT (K) ⟶
400
300
200
100
-0.5
0
0.5
1
15
1.5
25
grain refinement →
c_f=0.3
50
1.0
d_k=250 nm
100
U=ΔUSE/USE$_o$ ⟶

Fig. 7b

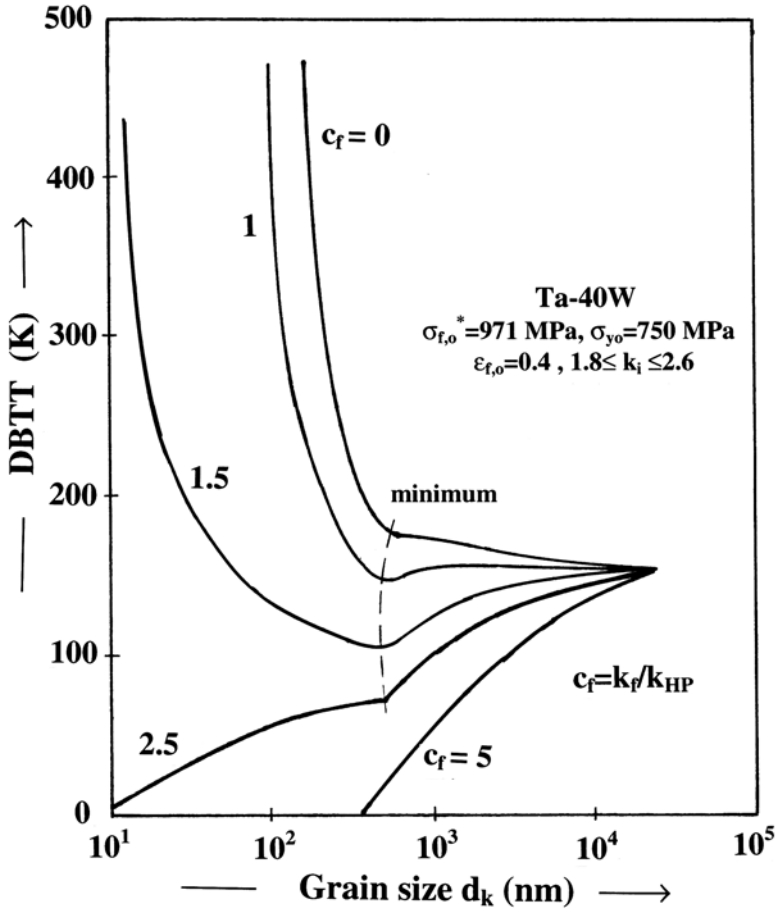
500
400
300
200
100
0
DBTT (K) ⟶
$c_f = 0$
1
1.5
2.5
$c_f = 5$
minimum
Ta-40W
$\sigma_{f,o}^*$=971 MPa, σ_{yo}=750 MPa
$\varepsilon_{f,o}$=0.4 , 1.8≤ k_i ≤2.6
$c_f = k_f/k_{HP}$
10^1
10^2
10^3
10^4
10^5
Grain size d_k (nm) ⟶

Fig. 8a

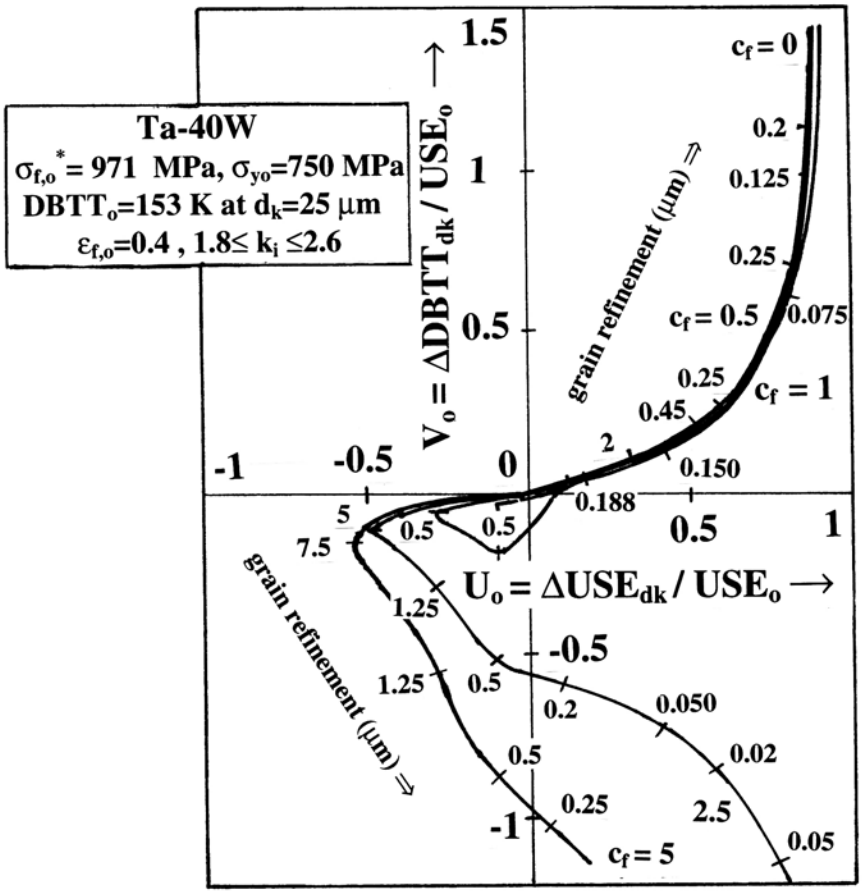
Ta-40W
$\sigma_{f,o}^*$ = 971 MPa, σ_{yo}=750 MPa
$DBTT_o$=153 K at d_k=25 μm
$\varepsilon_{f,o}$=0.4 , 1.8≤ k_i ≤2.6
$V_o = \Delta DBTT_{dk} / USE_o$ ⟶
$U_o = \Delta USE_{dk} / USE_o$ ⟶
grain refinement (μm) ⇒
grain refinement (μm) ⇒
$c_f = 0$
$c_f = 0.5$
$c_f = 1$
$c_f = 5$
1.5
1
0.5
-0.5
-1
0
0.5
1
0.2
0.125
0.25
0.075
0.45
2
0.150
0.188
5
7.5
1.25
0.050
0.02
2.5
0.05

Fig. 8b

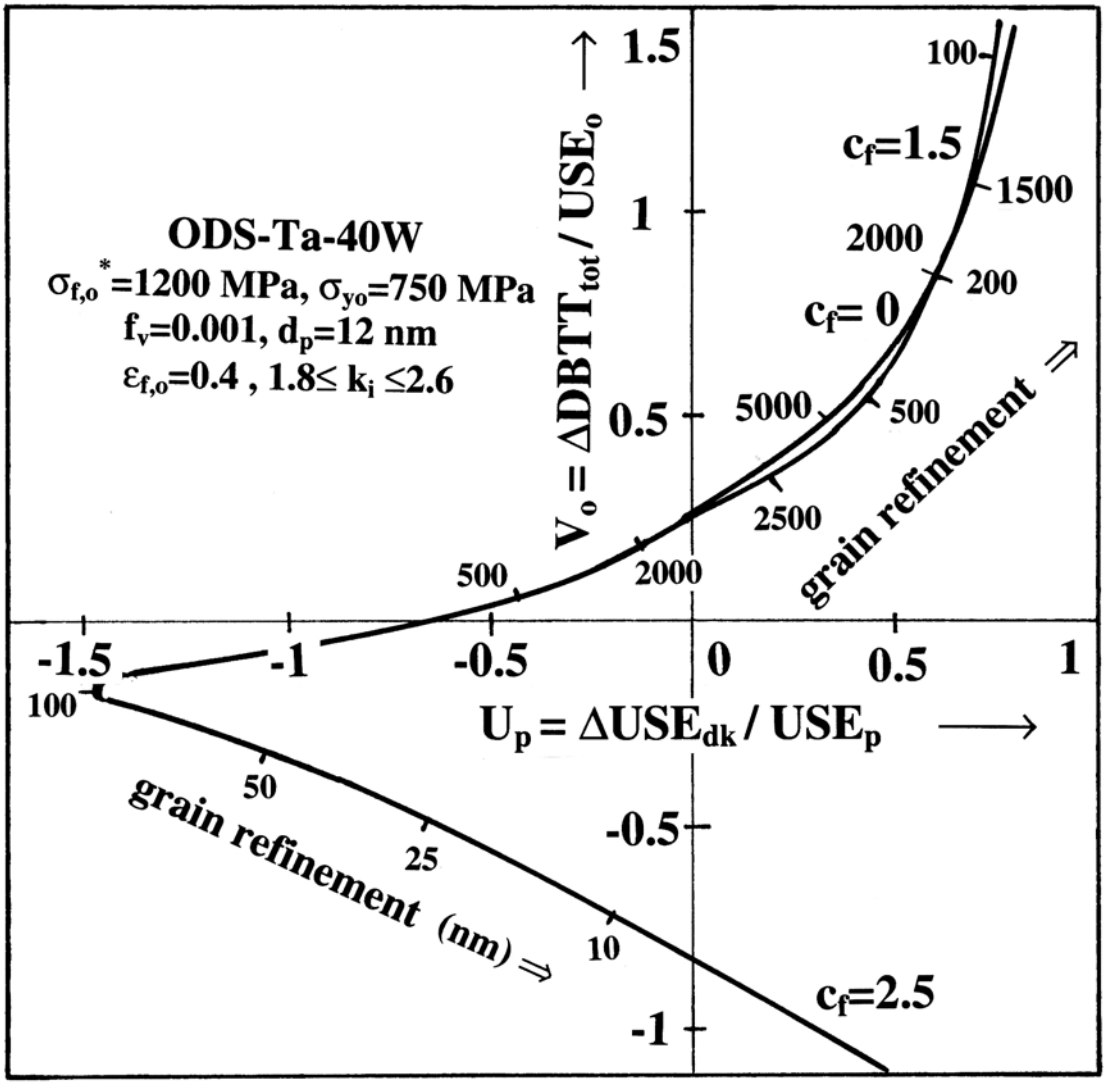
ODS-Ta-40W
$\sigma_{f,o}^*$=1200 MPa, σ_{yo}=750 MPa
f_v=0.001, d_p=12 nm
$\varepsilon_{f,o}$=0.4 , 1.8≤ k_i ≤2.6
$V_o = \Delta DBTT_{tot} / USE_o$
$U_p = \Delta USE_{dk} / USE_p$
c_f=1.5
c_f= 0
c_f=2.5
grain refinement ⇒
grain refinement (nm) ⇒
1.5
1
0.5
-0.5
-1
-1.5
0
0.5
100
1500
2000
200
5000
500
2500
500
2000
100
50
25
10

Fig. 9

Fig. 10

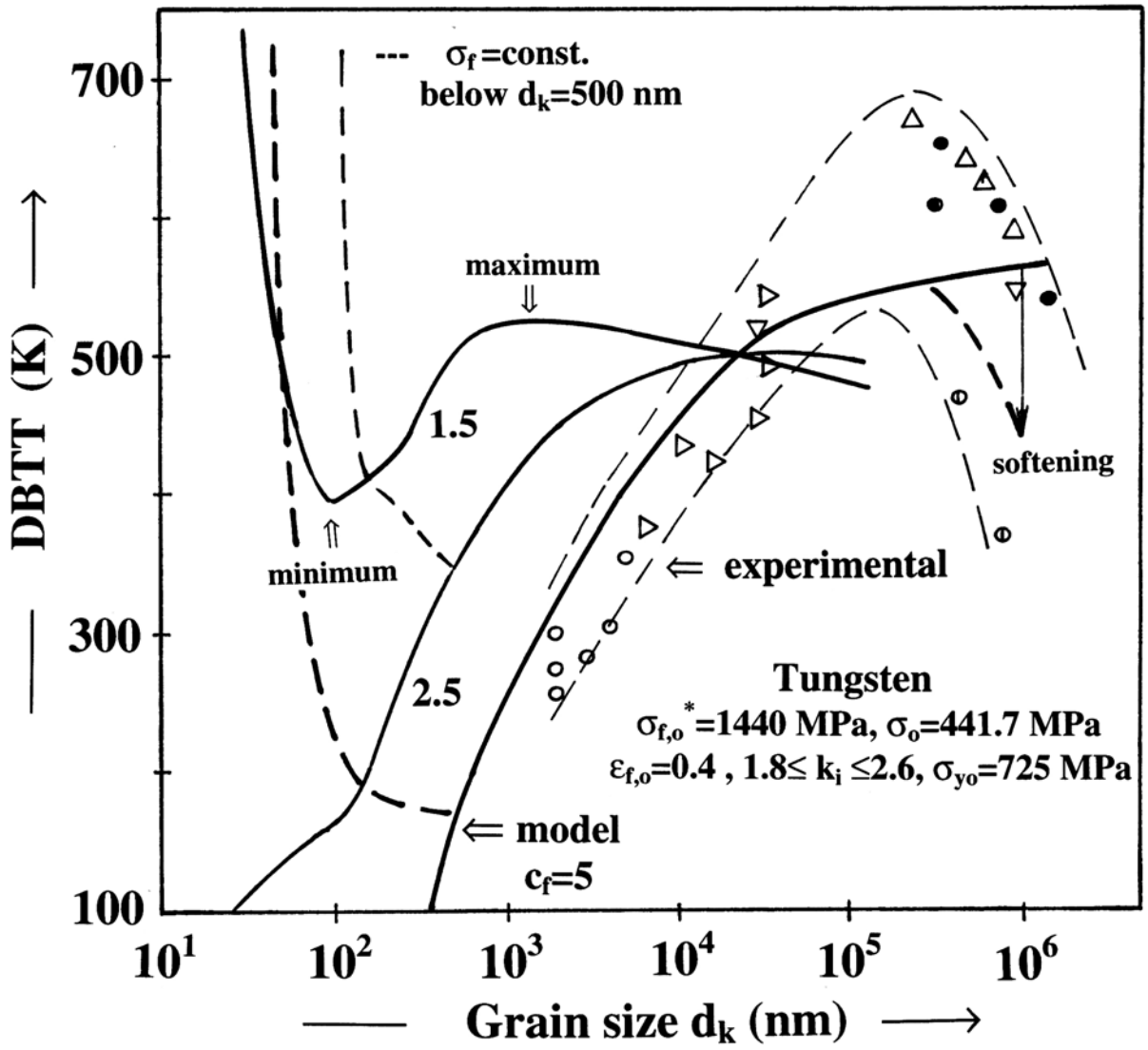
--- σ_f=const.
below d_k=500 nm
maximum
minimum
1.5
2.5
softening
⇐ experimental
⇐ model
c_f=5
Tungsten
$\sigma_{f,o}^*$=1440 MPa, σ_o=441.7 MPa
$\varepsilon_{f,o}$=0.4 , 1.8≤ k_i ≤2.6, σ_{yo}=725 MPa
DBTT (K) ⟶
700
500
300
100
10^1
10^2
10^3
10^4
10^5
10^6
Grain size d_k (nm) ⟶

Metal	b (nm)	μ (GPa)	T_m (°C)	Λ_{th} ($Wcm^{-1}K^{-1}$)	α_{th} (10^{-6})	Θ barns	decay time of main isotopes
α-Fe	0.2482	71.8	1536	0.804	11.8	2.3	45 d
Ta	0.2860	61.8	2996	0.575	6.3	5.5	114 d
W	0.2739	160.6	3387	1.73	4.5	5.5	75 d
Mo	0.2728	136.3	2610	1.38	4.8	3	66 h
Cr	0.2498	115.7	1875	0.939	4.9	2.5	28 d
Ta-40W	0.2812	101.3	3152	1.037	5.58	5.5	98 d

Tab. 1: Main physical properties of Ta, W, Ta-40at%W and Mo, Cr which compared with α-Fe.(d.. days, h…hours, Θ..cross section for ^{14}MeV neutrons)